

1 **Title**

2 Disease-associated regulatory variation often displays plasticity or temporal-specificity in fetal pancreas

3 **Authors**

4 Jennifer P. Nguyen^{1,2}, Timothy D. Arthur^{2,3}, Kyohei Fujita⁴, Bianca M. Salgado⁴, Margaret K.R. Donovan^{1,2}, iPSCORE
5 Consortium⁵, Hiroko Matsui⁴, Agnieszka D’Antonio-Chronowska^{6*}, Matteo D’Antonio^{2*}, Kelly A. Frazer^{4,6*}

6 Affiliations:

7 ¹ Bioinformatics and Systems Biology Graduate Program, University of California, San Diego, La Jolla, CA, 92093,
8 USA

9 ² Department of Biomedical Informatics, University of California, San Diego, La Jolla, CA, 92093, USA

10 ³ Biomedical Sciences Graduate Program, University of California, San Diego, La Jolla, CA 92093, USA

11 ⁴ Institute of Genomic Medicine, University of California San Diego, 9500 Gilman Dr, La Jolla, CA, 92093, USA

12 ⁵ A full list of Consortium members and their affiliations appears at the end of the manuscript

13 ⁶ Department of Pediatrics, University of California, San Diego, La Jolla, CA, 92093, USA

14 * Correspondence to: Agnieszka D’Antonio-Chronowska (adc055@health.ucsd.edu); Matteo D’Antonio
15 (madantonio@health.ucsd.edu); Kelly A. Frazer (kafrazer@health.ucsd.edu).

16 **Abstract**

17 The role of genetic regulatory variation during fetal pancreas development is not well understood. We generate a panel
18 of 107 fetal-like iPSC-derived pancreatic progenitor cells (iPSC-PPCs) from whole genome-sequenced individuals and
19 identify 4,065 genes and 4,016 isoforms whose expression and/or alternative splicing are affected by regulatory
20 variation. We integrate endocrine and exocrine eQTLs identified in adult pancreatic tissues, which reveals 2,683 eQTL
21 associations that are unique to the fetal-like iPSC-PPCs and 1,139 eQTLs that exhibit regulatory plasticity across fetal-
22 like and adult pancreas. Investigation of GWAS risk loci for pancreatic diseases shows that some putative causal
23 regulatory variants are active in the fetal-like iPSC-PPCs and likely influence disease by modulating expression of
24 disease-associated genes in early development, while others with regulatory plasticity can exert their effects in both
25 the fetal and adult pancreas by modulating expression of different disease genes in the two developmental stages.

26 **Introduction**

27 Genome-wide association studies (GWAS) have identified hundreds of genetic variants associated with pancreatic
28 disease risk and phenotypes¹⁻⁴. However, the majority of these associations map predominantly to non-coding regions
29 of the genome, thereby hindering functional insights to disease processes⁵⁻⁷. Previous large-scale expression
30 quantitative trait loci (eQTL) studies have made significant advancements towards understanding how genetic variation
31 affects gene expression in various tissues and cell types, as well as their contribution to human traits and diseases⁸⁻¹¹.
32 However, these analyses have been limited to adult tissues and therefore do not capture the effects of regulatory
33 variation on gene expression under fetal conditions. In addition, integration of fetal and adult eQTL datasets will enable
34 the investigation of regulatory plasticity of genetic variants, which refers to changes in variant function under different
35 spatiotemporal contexts^{9,12,13}. Understanding how genetic variation affects gene expression during early pancreas
36 development, and how their function changes in adulthood, could expand our understanding of the biological
37 mechanisms underlying adult pancreatic disease and GWAS complex trait loci.

38 Many lines of evidence from clinical and genomic studies indicate an important role of pancreatic development to the
39 health and childhood and adult onset pancreatic diseases^{12,13,14,15}. For example, mutations in genes critical to pancreatic
40 development, such as *PDX1*, *HNF4A*, and *HNF1A*, are associated with childhood onset diabetes¹⁸⁻²⁰. Furthermore,
41 type 2 diabetes (T2D)-risk variants map to transcription factors (TFs) that are crucial to pancreatic development,
42 including *NEUROG3* and *HNF1A*, and are enriched in accessible pancreatic progenitor-specific enhancers^{4,21}. To
43 address the limited availability of fetal pancreatic tissues, protocols have been devised to efficiently guide the
44 differentiation of human induced pluripotent stem cells (iPSCs) into pancreatic progenitor cells (iPSC-PPCs) as a
45 model system to study the fetal pancreas²²⁻²⁷. While this model system has expanded our knowledge of pancreatic
46 developmental biology, an eQTL study in this fetal-like pancreatic developmental stage, which requires hundreds of
47 well-characterized iPSC-PPCs derived from different individuals, has not yet been conducted.

48 In this study, we derived and characterized a large resource of iPSC-PPCs and conducted an eQTL analysis to map
49 genetic loci associated with gene expression and isoform usage in fetal-like pancreatic cells. We integrated eQTLs
50 from adult pancreatic tissues and identified eQTL loci that displayed temporal-specificity in early pancreatic
51 development, as well as loci that were shared with adult but displayed regulatory plasticity. Annotation of GWAS risk
52 loci using our temporally informed eQTL resource revealed causal regulatory variants with developmental-specific
53 effects associated with complex pancreatic traits and disease.

54 **Results**

55 **Overview of study**

56 The goal of our study is to understand how regulatory variation active in early pancreatic development influences
57 pancreatic disease risk and phenotypes (Figure 1A). We differentiated 106 iPSC lines from the iPSCORE resource
58 derived from 106 whole-genome sequenced individuals to generate 107 iPSC-PPC samples (one iPSC line was
59 differentiated twice) (Figure S1, Table S1, Table S2). We characterized the fetal-like pancreatic transcriptome as well
60 as cellular composition using single-cell RNA-seq (scRNA-seq) of eight iPSC-PPC samples. Then, we conducted an
61 eQTL analysis on bulk RNA-seq of all 107 samples to identify regulatory variants associated with fetal-like gene
62 expression and isoform usage. To understand the developmental-specificity and regulatory plasticity of genetic
63 variants, we integrated eQTLs previously discovered in adult pancreatic endocrine and exocrine samples using
64 colocalization and network analysis. Finally, using our eQTL resource of pancreatic tissues (i.e., fetal-like iPSC-
65 derived PPCs, adult endocrine, adult exocrine), we performed GWAS colocalization and fine-mapping to link
66 regulatory mechanisms and identify putative causal variants underlying pancreatic traits and disease associations.

67 **Large-scale differentiation of fetal-like pancreatic progenitor cells**

68 To assess differentiation efficiency of the 107 iPSC-PPCs, we performed flow cytometry analysis on each sample for
69 the expression of PDX1 and NKX6-1, two markers routinely assayed for early pancreatic progenitor formation. Across
70 the 107 samples, we observed a median percentage of PDX1⁺ cells of 92.1%, indicating that the majority of the cells
71 in iPSC-PPCs had differentiated towards pancreas lineage (Figure 1B, Figure S2, Table S2). Pancreatic progenitor cells
72 that express PDX1 further differentiate into pancreatic endoderm, which expresses both PDX1 and NKX6-1 and gives
73 rise to both endocrine and exocrine pancreatic cell types²⁸. Therefore, to determine the fraction of PPCs that
74 differentiated into pancreatic endoderm (hereafter referred to as “late PPC”), we examined the percentage of cells
75 expressing both PDX1 and NKX6-1 across the 107 iPSC-PPCs and found that the median percentage of PDX1⁺/NKX6-
76 1⁺ cells was 74% (range: 9.4%-93.1%), whereas the median percentage of cells that expressed PDX1 but not NKX6-1
77 (PDX1⁺/NKX6-1⁻, hereafter referred to as “early PPC”) was 18.7% (range: 3.5-59.3%, Figure 1B, Figure S2, Table
78 S2). Consistent with flow cytometry analysis, scRNA-seq of ten derived iPSC-PPCs confirmed the presence of both
79 early and late PPCs and that the majority of the cells were late PPCs (Figure S3-8; Table S2-4; See Methods and
80 Supplemental Note 1). Altogether, these results show that the majority of the cells in iPSC-PPCs have differentiated
81 into pancreatic endoderm while a smaller fraction represented a primitive PPC state.

82 To examine the similarities between iPSC-PPC and adult pancreatic transcriptomes, we generated bulk RNA-seq for
83 all 107 iPSC-PPC samples and inferred the pseudotime on each sample, along with 213 iPSCs^{29,30}, 87 pancreatic islets

84 ³¹, and 176 whole pancreatic tissues ³². Because pancreatic islets consist primarily of endocrine cells, and whole
85 pancreas samples consist primarily of exocrine cells, we hereafter refer to these tissues as “adult pancreatic
86 endocrine” and “adult pancreatic exocrine”, respectively. Pseudotime analysis revealed that iPSC-PPC samples
87 represented an intermediate stage between iPSCs and the adult pancreatic tissues, confirming that iPSC-PPC
88 corresponded to an earlier developmental timepoint compared to the adult tissues (Figure S9, Table S5).

89 These analyses, combined with the results of previous studies ^{23,26,33}, show that the 107 derived iPSC-PPCs represent a
90 fetal-like state of pancreatic tissues, containing both pancreatic endocrine and exocrine progenitor cells.

91 **Identification and characterization of gene and isoform eQTLs in fetal-like iPSC-PPCs**

92 To characterize the effects of genetic variation on the fetal-like iPSC-PPC transcriptome, we performed an eQTL
93 analysis mapping the genetic associations with fetal-like gene expression (e_g QTL) and relative isoform usage (e_i QTL).
94 Considering only autosomal chromosomes, we analyzed a total of 16,464 genes and 29,871 isoforms (corresponding
95 to 9,624 autosomal genes) that were expressed in the fetal-like iPSC-PPCs (for genes ≥ 1 TPM in at least 10% of the
96 samples or for isoforms $\geq 10\%$ usage in at least 10% of samples). We identified 4,065 (24.7%) eGenes and 4,016
97 (13.0%) eIsoforms with an e_g QTL or e_i QTL, respectively (FDR < 0.01 , Figure 1C-D, Table S6). To detect additional
98 independent eQTL signals ³⁴, we performed a stepwise regression analysis to identify additional independent eQTLs
99 (i.e., conditional eQTLs) for each eGene and eIsoform, and yielded 368 e_g QTLs (mapping to 338 eGenes) and 216
100 e_i QTLs (mapping to 198 eIsoforms), totaling to 4,433 independent e_g QTL associations and 4,232 independent e_i QTL
101 associations (Figure 1C-D, Table S6). We next predicted candidate causal variants underlying each eQTL (e_g QTL and
102 e_i QTL) association using genetic fine-mapping ³⁵ (Table S7) and tested their enrichments in transcribed regions and
103 regulatory elements. We observed an enrichment of e_g QTLs in intergenic and promoter regions while e_i QTLs were
104 enriched in splice sites and RNA-binding protein binding sites (Figure 1E). We additionally estimated the transcription
105 factor (TF) binding score on each variant using the Genetic Variants Allelic TF Binding Database ³⁶ and found that, at
106 increasing posterior probability (PP) thresholds, the candidate causal variants underlying e_g QTLs were more likely to
107 affect TF binding compared to those underlying e_i QTLs (Figure 1F, Table S7, Table S8). These results corroborate
108 similar findings from previous studies ^{10,12,37} showing that the genetic variants underlying e_g QTLs primarily affect gene
109 regulation and e_i QTLs primarily affect coding regions or alternative splicing.

110 To further characterize the function of genetic variants associated with the fetal-like iPSC-PPC transcriptome, we
111 examined the distributions of e_g QTLs and e_i QTLs per gene. Of the 5,169 genes whose phenotype was affected by
112 genetic variation, 1,008 were impacted through both gene expression and isoform usage (i.e., had both e_g QTL and
113 e_i QTLs, 17.9%) while 3,057 were impacted through only gene expression (i.e., had only e_g QTLs, 53.6%) and 1,554
114 through only isoform usage (i.e., had only e_i QTLs, 27.7%, Figure 1G, Table S6). For the 1,008 genes with both e_g QTL
115 and e_i QTLs, we examined whether the same or different genetic variants underpinned their associations using

116 colocalization. We identified 410 (40.7%) genes that had at least one H4 (model for shared causal variants; $PP.H4 \geq$
117 80%) or H3 (model for distinct causal variants; $PP.H3 \geq 80\%$) association between their e_g QTL and e_i QTLs, of which
118 the majority (333, 81.2%) had only overlapping signals (all H4), 38 (9.3%) had only non-overlapping signals (all H3),
119 and 39 (9.5%) had both overlapping and non-overlapping e_i QTLs (both H3 and H4; an e_g QTL can overlap with an
120 e_i QTL corresponding to one isoform but not with another e_i QTL corresponding to a second isoform) (Figure 1G, Table
121 S9). The remaining 598 genes had $PP.H3 < 80\%$ and $PP.H4 < 80\%$ due to insufficient power (Figure 1G). Enrichment
122 analysis of overlapping e_g QTL and e_i QTLs showed that these variants likely disrupt mechanisms affecting both gene
123 expression and alternative splicing (Figure S10). These findings show that 17.9% of genes had both e_g QTLs, and
124 e_i QTLs and that their effects were commonly driven by the same causal variants while a fraction were driven by different
125 causal variants. Overall, our results show that the majority of genes had either only e_g QTLs or e_i QTLs, indicating that
126 the functional mechanisms underlying these associations are likely independent where genetic variants affecting
127 alternative splicing does not affect the overall expression of the gene, and vice versa.

128 **Most fetal-like and adult endocrine eGenes show developmental stage specificity**

129 Studies aimed at identifying and characterizing eGenes have been conducted in both adult pancreatic endocrine and
130 exocrine tissues ^{8,10,11,31,38}; however, the endocrine tissue has been more thoroughly studied because of its role in
131 diabetes. Therefore, we focused on understanding the similarities and differences between eGenes in the fetal-like
132 iPSC-PPCs and adult pancreatic endocrine tissues.

133 We obtained eQTL summary statistics and intersected the 4,211 autosomal eGenes identified in 420 adult pancreatic
134 endocrine samples ¹¹ with the 4,065 eGenes in fetal-like iPSC-PPC. We found that only 1,501 (36.9% of 4,065) eGenes
135 overlapped between the fetal-like iPSC-PPC and adult endocrine tissues (Figure 2A). To determine whether the small
136 overlap was due to gene expression differences, we examined how many of the eGenes were expressed in both the
137 fetal-like iPSC-PPC and adult pancreatic endocrine. Of the 4,065 fetal-like iPSC-PPC eGenes, 88.7% (3,605) were
138 also expressed in adult endocrine samples; likewise, of the 4,211 adult endocrine eGenes, 78.4% (3,301) were also
139 expressed in the fetal-like iPSC-PPCs (Figure 2A). These results suggest that most fetal-like iPSC-PPC eGenes were
140 expressed but not associated with genetic variation in the adult endocrine samples, and vice versa.

141 For eGenes that were present in both the fetal-like iPSC-PPC and adult endocrine samples, we next asked whether their
142 expression were controlled by the same genetic variants. We performed colocalization between e_g QTLs for the 1,501
143 shared eGenes in the fetal-like iPSC-PPC and adult endocrine, and found that 795 (52.3%) had either a H4 or H3
144 association ($PP.H4$ or $PP.H3 \geq 80\%$) (Table S9). Of the 795 with an association, 701 (88.2%) had overlapping e_g QTL
145 signals ($PP.H4 \geq 80\%$) while 94 (11.8%) had non-overlapping e_g QTL signals ($PP.H3 \geq 80\%$) (Figure 2B, Table S9).
146 These results indicate that most shared eGenes were associated with the same genetic variants controlling their gene
147 expressions in both fetal-like and adult pancreatic endocrine tissues, while a subset had non-overlapping genetic

148 variants. For example, we identified *SNX29* as an eGene in both fetal-like iPSC-PPC and adult pancreatic endocrine
149 but observed that its expression was associated with distinct eQTL signals approximately 520 kb apart (Figure 2C).
150 *SNX29* is involved in various signaling pathways³⁹, including TGF- β , ErbB, and WNT signaling pathway, and
151 predicted to be a causal gene for body-mass index (BMI) and T2D⁴⁰.

152 Taken together, our results show that a minor proportion of fetal-like eGenes (1,501, 37%) were shared with adult
153 endocrine tissues, whereas ~63% (2,564) were fetal development-specific; and, while most shared eGenes are
154 associated with the same regulatory variants, ~12% are mediated by different eQTLs. These findings support previous
155 observations that the chromatin landscape differs between fetal and adult involving developmental-specific enhancer-
156 promoter interactions⁴¹⁻⁴³.

157 **Identification of developmental-unique and shared e_gQTLs**

158 Above, we described eGenes that were unique to fetal-like or adult endocrine, or shared between both pancreatic
159 tissues. Here, we sought to identify eQTLs (i.e., regulatory variants) that specifically affect gene expression during
160 pancreas development, in adult stage, or both stages. Because the iPSC-PPCs give rise to both endocrine and exocrine
161 cell fates, we included eQTLs from both adult pancreatic endocrine¹¹ and pancreatic exocrine³² tissues in our analyses.
162 Due to the many different types of eQTLs used in this study, we refer to all eQTLs as a collective unit as “eQTLs”,
163 eQTLs that were associated with gene expression as “e_gQTLs”, and eQTLs associated with changes in alternative
164 splicing (e_iQTLs, exon eQTLs, and sQTLs) as “e_{AS}QTLs”. For simple interpretations, we only describe the results for
165 the analyses conducted on the e_gQTLs below, however, we identified unique and shared iPSC-PPC e_{AS}QTL
166 associations by conducting the same analyses (see Supplementary Note 2).

167 To identify e_gQTLs that shared the same regulatory variants, we performed pairwise colocalization using *coloc*³⁵
168 between e_gQTLs in fetal-like iPSC-PPC, in adult endocrine¹¹, and in adult exocrine pancreatic samples¹⁰. We
169 considered e_gQTLs that had at least one variant with causal PP $\geq 1\%$, outside the MHC region, and associated with
170 genes annotated in GENCODE version 34⁴⁴ (see Methods). We retained 4,149 fetal-like iPSC-PPC e_gQTLs, 3,948
171 adult endocrine e_gQTLs, and 8,312 adult exocrine e_gQTLs for downstream analyses (Table S10). We identified 7,893
172 total pairs of e_gQTLs that shared the same signal (PP.H4 $\geq 80\%$), which comprised 7,839 e_gQTLs (1,630 iPSC-PPC,
173 2,417 adult endocrine, and 3,792 adult exocrine; Figure S11A). Of the 7,893 pairs, 27.3% (2,157) were between pairs
174 of e_gQTLs within the same pancreatic tissue associated with the expression of different eGenes and 72.7% (5,736) were
175 between pairs of e_gQTLs active in two different pancreatic tissues (Figure S11B, Table S9). Of the 5,736 e_gQTL pairs,
176 43.5% (2,496) were associated with the expression of the same eGene in the two tissues while 56.5% (3,240) were
177 associated with different eGenes (Figure S11B). Interestingly, we observed 1,301 iPSC-PPC, 902 adult endocrine, and
178 2,574 adult exocrine e_gQTLs that did not colocalize and were not in LD ($r^2 \geq 0.2$ and within 500 Kb) with nearby
179 e_gQTLs, suggesting that the underlying genetic variants were associated with a single eGene and active only either

180 during early pancreas development or in a specific adult pancreatic tissue (Figure 3A, Table S10). Hereafter, we refer
181 to eQTLs that did not colocalize with another eQTL and were not in LD with nearby eQTLs as “singletons” (i.e., such
182 as the 1,301 iPSC-PPC, 902 adult endocrine, and 2,574 adult exocrine e_gQTLs described above) and those that
183 colocalized with another eQTL (same or different tissue) as “combinatorial” (i.e., such as the 7,839 e_gQTLs described
184 above). Given that singleton e_gQTLs were active in only the corresponding pancreatic tissue, singleton e_gQTLs were
185 by-definition tissue-unique.

186 To identify combinatorial eQTL signals that were unique or shared between the three pancreatic tissues, we performed
187 network analysis using the 7,893 pairs of colocalized e_gQTL associations to identify modules of e_gQTLs, which we
188 defined as an eQTL signal that was either associated with multiple genes in a single tissue, or one or more genes in at
189 least two of the three different pancreatic tissues. We identified 1,974 e_gQTL modules in total, of which 1,023 (51.8%)
190 were composed of two e_gQTLs while the remaining 951 (48.2%) had an average of four e_gQTLs per module (range: 3-
191 20 e_gQTLs) (Table S10, Table S11). We found that 237 (12.0% of 1,974) modules were tissue-unique (i.e., contained
192 only e_gQTLs from one tissue and not in LD [$r^2 \geq 0.2$ and within 500 Kb] with nearby eQTLs in the other two tissues),
193 of which 17 were fetal-like iPSC-PPC-unique, 37 adult endocrine-unique, and 183 adult exocrine-unique, and
194 altogether comprised 35, 77, and 415 combinatorial e_gQTL associations, respectively (Figure 3A, Figure 3B, Table
195 S10, Table S11). In contrast, the remaining 1,737 (88.0% of 1,974) modules were associated with multiple pancreatic
196 tissues, of which 702 were shared between only adult pancreatic endocrine and exocrine tissues (referred to as “adult-
197 shared”), 74 were shared between only iPSC-PPC and adult endocrine (“fetal-endocrine”), 309 between only iPSC-
198 PPC and adult exocrine (“fetal-exocrine”), and 652 between all three pancreatic tissues (“fetal-adult”) (Figure 3B,
199 Table S10, Table S11). Together, the 1,035 (74 + 309 + 652) modules shared between iPSC-PPC and an adult
200 pancreatic tissue were composed of 1,241 iPSC-PPC, 945 adult endocrine, and 1,440 adult exocrine e_gQTLs (Table
201 S10, Table S11).

202 Altogether, we identified 1,336 (32.2% of 4,149) e_gQTLs that were unique to fetal-like iPSC-PPC, of which 1,301
203 functioned as singletons and 35 in modules, while 1,241 (29.9% of 4,149) e_gQTLs were shared with adult pancreatic
204 tissues (Table S10, Table S11). The remaining iPSC-PPC e_gQTLs (1,572, 37.9% of 4,149) were annotated as
205 “ambiguous” and excluded from downstream analyses due to potential associations with adult e_gQTLs based on LD
206 and/or not meeting thresholds for module identification (see Methods, Table S10, Table S11). Our results show that
207 the vast majority of iPSC-PPC-unique regulatory variants were singletons while combinatorial e_gQTLs tended to be
208 shared across pancreatic tissues and sometimes were associated with different eGenes. For e_{AS}QTLs, we observed
209 similar trends in which the majority of iPSC-PPC-unique e_{AS}QTLs were singletons and that combinatorial e_{AS}QTLs
210 were likely shared and potentially with different genes (see Supplemental Note 2; Figure S12, Table S9, Table S10).

211 **Functional validation and characterization of tissue-unique e_gQTLs**

212 To functionally characterize singleton and combinatorial tissue-unique e_g QTLs, we examined their enrichments in
213 chromatin states defined in all three pancreatic tissues^{7,21,45}. We observed that all three tissue-unique singleton e_g QTLs
214 were enriched in active chromatin regions in their respective tissues, including enhancers, promoters, and the sequences
215 corresponding to flanking promoters (Figure 3C, Figure S11C, Table S12). Adult endocrine-unique and exocrine-
216 unique combinatorials were also enriched in active chromatin states but had stronger preferences for enhancers, which
217 is consistent with the characteristic of enhancers in regulating multiple genes (Figure 3C, Figure S11C, Table S12). Of
218 note, iPSC-PPC-unique combinatorial e_g QTLs were enriched in quiescent and genic enhancer regions in adult
219 endocrine. Similarly, adult endocrine- and exocrine-unique singleton e_g QTLs were enriched in active regulatory
220 regions in PPC but were not detected as e_g QTLs in iPSC-PPC. For example, in the chr2:198053627-198143627 locus
221 overlapping an active PPC enhancer, we observed that the variants were associated with an e_g QTL signal only in adult
222 endocrine (Figure S11D). For these e_g QTLs that overlap an active regulatory element in a different tissue but do not
223 affect gene expression, it may be possible that these variants act through the disruption of tissue-unique TF binding⁴³.
224 Altogether, our results demonstrate that tissue-unique singleton and combinatorial e_g QTLs were strongly enriched for
225 active chromatin regions with combinatorial e_g QTLs having the strongest preference for enhancers as observed in adult.

226 Here, we present three examples of tissue-unique e_g QTL modules that illustrate context-specificity of genetic variants
227 in the three pancreatic tissues. We identified the e_g QTL module GE_3_1 (“GE” means that this module is associated
228 with gene expression) as a fetal-unique e_g QTL locus (chr3:148903264-148983264) because the underlying genetic
229 variants were associated with *CP* and *HPS3* expression in only iPSC-PPC while in adult endocrine and exocrine
230 pancreas, the variants were not detected as e_g QTLs (Figure 3D-E). Similarly, GE_15_13 was an adult endocrine-unique
231 e_g QTL locus (chr15:57746360-57916360) associated with *GCOM1*, *MYZAP*, and *POLR2M* expression, while in the
232 other two pancreatic tissues, the variants were inactive and not associated with gene expression (Figure 3F-G). Finally,
233 we discovered GE_5_32 as an adult exocrine-unique e_g QTL locus (chr5:146546063-146746063) associated with
234 *STK32A* and *STK32A-AS1* expression in only the adult pancreatic exocrine (Figure 3H-I). Together, these results show
235 that gene regulation varies between fetal-like and adult pancreatic stages, as well as between the two adult tissues,
236 further demonstrating the importance of profiling different spatiotemporal contexts of the pancreas to delineate
237 molecular mechanisms underlying pancreatic disease.

238 **Regulatory plasticity in e_g QTL signals shared between fetal-like and adult pancreatic tissues**

239 Above, we demonstrated that genetic variants can exhibit temporal-specificity between fetal-like and adult tissues.
240 Next, we sought to examine regulatory variants that are shared between the two stages and understand how their
241 function changes. Using the 1,035 e_g QTL modules shared between fetal-like iPSC-PPC and adult pancreatic tissues,
242 we next sought to understand how genetic variant function changes between the two developmental stages.
243 Specifically, we asked whether the underlying e_g QTL signals in the modules were associated with the same or different
244 eGenes in the three pancreatic tissues. We identified the following five categories (Figure 4A, Table S11): A) 230

245 (22.2%) e_gQTL modules were associated with same eGene(s) (range: 1-2) between fetal-like iPSC-PPC and only one
246 of the two adult pancreatic tissues; B) 305 (29.5%) were associated with the expression of the same eGene(s) (range
247 1-2) in the fetal-like and both adult tissues; C) 363 (35.1%) were associated with 2-9 eGenes, some of which were
248 shared, but at least one eGene was different between the fetal-like and at least one of the adult tissues (referred to as
249 “partial overlap”); D) 97 (9.4%) were associated with different eGenes (range: 2-5) between fetal-like iPSC-PPCs and
250 one of the two adult pancreatic tissues; and E) the remaining 40 (3.9%) were associated with different eGenes (range:
251 2-8) between the fetal-like and both adult endocrine and exocrine tissues (i.e., there is no overlap of eGenes between
252 the two developmental stages).

253 Here, we illustrate examples of e_gQTL modules in three intervals to highlight how eQTL associations varied between
254 fetal-like and adult states. In the chr11:111505862-112155862 locus, we discovered a fetal-adult e_gQTL module
255 (GE_11_69) that comprised e_gQTL associations with different eGenes in iPSC-PPC and the two adult pancreatic
256 tissues, specifically *CRYAB* in iPSC-PPC and *C11orf1* in the two adult tissues (Figure 4B). Likewise, the
257 chr19:4213666-4433666 locus corresponding to a fetal-adult e_gQTL module (GE_19_90) was associated with *MPND*
258 expression in only iPSC-PPC but in adult pancreatic endocrine and exocrine, the underlying variants were associated
259 with *STAP2* expression (Figure 4C). Finally, the fetal-adult e_gQTL locus (GE_10_11) in chr10:1273918-1276118
260 affected *URO5* expression in all three pancreatic tissues but in adult pancreatic endocrine, the underlying variants also
261 affected *BCCIP* expression (Figure 4D). Together, these genomic loci illustrate examples of regulatory plasticity
262 observed in genetic variants in which their genotypes incur different transcriptional phenotypes depending on the life
263 stage of the pancreas.

264 Taken together, our findings reveal that 48.3% of shared e_gQTL loci (n = 500; categories C-E) comprising 691 iPSC-
265 PPC, 578 adult endocrine, and 959 adult exocrine e_gQTL associations display regulatory plasticity in which the
266 underlying regulatory variants are associated with one or more different eGenes and could thereby affect different
267 biological processes. For e_{AS}QTLs, we found that 39.8% e_{AS}QTL loci (n = 208; categories C-E) are shared between
268 fetal-like and adult pancreas and associated with multiple different genes, comprising 448 iPSC-PPC, 384 adult
269 endocrine, and 217 adult exocrine e_{AS}QTLs (see Supplemental Note 2).

270 **Associations of developmental stage-unique eQTLs with pancreatic traits and disease** 271 **phenotypes**

272 To better understand the role of regulatory variants associated with complex human traits and disease during early
273 development and adult pancreatic stages, we performed colocalization between GWAS signals and eQTLs (e_gQTL and
274 e_{AS}QTL) detected in fetal-like iPSC-PPC, adult endocrine, and adult exocrine tissues. For this analysis, we considered
275 GWAS data from ten different studies for two diseases involving the pancreas, including type 1 diabetes (T1D)³ and
276 type 2 diabetes (T2D)⁴, and seven biomarkers related to three traits: 1) glycemic control (HbA1c levels and fasting

277 glucose)^{2,46}; 2) obesity (triglycerides, cholesterol, HDL level, and LDL direct)⁴⁶; and 3) body mass index (BMI)⁴⁶
278 (Table S13).

279 *Singleton eQTLs*

280 Out of the 8,137 singleton eQTLs (4,777 e_gQTLs and 3,360 e_{AS}QTLs see Supplemental Note 2) in the fetal-like iPSC-
281 PPC and two adult pancreatic tissues, we found 164 (2%) that displayed strong evidence for colocalization with at least
282 one GWAS signal, including 30 (of 2,205 total singleton eQTLs; 1.4%) fetal-like iPSC-PPC, 71 (of 2,705; 2.6%) adult
283 endocrine, and 63 (of 3,227; 2.0%) adult exocrine singleton eQTLs (Figure 5A, Figure S13, Table S13). Given that
284 some traits are highly correlated with one another^{47,48}, we observed 49 eQTLs that colocalized with GWAS variants
285 associated with more than one trait (average: 1.5 traits per singleton eQTL; range: 1-6 studies). In total, we identified
286 248 GWAS loci (across the ten GWAS studies) that displayed colocalization with fetal-like or adult pancreatic
287 singleton eQTLs (Table S13). We next identified putative causal variants underlying both eQTL and trait associations
288 and constructed 99% credible sets where the cumulative causal PP > 99% (see Methods). Of the total 248 GWAS loci,
289 we were able to resolve 34 loci to a single putative causal variant while 84 had between two and ten variants and the
290 remaining 130 had more than ten variants with an average of ~45 variants per locus (Figure 5B, Table S14).

291 *eQTL modules*

292 We next analyzed the combinatorial eQTLs (i.e., eQTLs that colocalize with one another) for GWAS colocalization.
293 We considered an eQTL module to overlap with GWAS variants if more than 30% of the eQTLs in the module
294 colocalized with PP.H4 > 80% and the number of H4 associations were twice greater than the number of H3
295 associations (see Methods). Of the 3,185 (1,974 e_gQTL and 1,211 e_{AS}QTL) modules, 105 (63 e_gQTL + 42 e_{AS}QTL;
296 3.3%) colocalized with a total of 149 GWAS signals (Table S13). Of these 105 GWAS-colocalized modules, 9 were
297 associated with only fetal-like iPSC-PPC eQTLs, 42 were shared between both iPSC-PPC and adult, (5 fetal-endocrine,
298 16 fetal-exocrine and 21 fetal-adult modules), and 54 were associated with only adult eQTLs (23 endocrine-unique, 8
299 exocrine-unique, 23 adult-unique) (Figure S13, Table S13). These 105 modules were composed of 49 iPSC-PPC
300 eQTLs, 84 adult endocrine eQTLs, and 49 adult exocrine eQTLs. Interestingly, we observed that all 9 of the fetal-
301 unique modules corresponded to e_{AS}QTL modules, which aligns with previous observations that alternative splicing is
302 overall more prominent in fetal compared with adult tissues and thus, tends to be highly developmental stage-specific
303⁴⁹. To obtain 99% credible sets for each of the 149 GWAS signals that colocalized with an eQTL module, we focused
304 on the eQTL association that resulted in the least number of putative causal variants (see Methods). 17 GWAS loci had
305 a credible set size of one variant, 58 with two to ten variants, and the remaining 74 had more than ten variants and an
306 average of ~34 variants per set (Figure 5C, Table S14).

307 In summary, we identified 79 eQTLs in iPSC-PPC (30 singleton + 49 combinatorial) that colocalized with GWAS
308 variants associated with complex pancreatic traits and disease, 30 of which we found to function as singleton eQTLs
309 (i.e., affect fetal-specific expression or alternative splicing of a single gene) while 49 were combinatorial eQTLs (i.e.,
10

310 affect expression or alternative splicing of multiple genes or isoforms). Of these combinatorial eQTLs, 16 were fetal-
311 unique (i.e., only colocalized with iPSC-PPC eQTLs) while 33 were adult-shared (i.e., colocalized with an adult
312 pancreatic eQTL). Furthermore, we observed that all 9 fetal-unique eQTL modules exclusively affected alternative
313 splicing, indicating that fetal-unique regulatory variants associated with disease may likely affect splice mechanisms
314 rather than gene transcription, consistent with previous studies demonstrating widespread alternative splicing during
315 embryonic development⁴⁹⁻⁵¹.

316 **Interpreting mechanisms of fine-mapped GWAS signals**

317 Fetal pancreatic tissues are not typically assessed for GWAS annotation, so the role of developmental regulatory
318 variants, and how their function changes in adult, is currently unclear. To better understand the function of disease-
319 associated variants in both fetal-like and adult pancreatic contexts, we used our previous assessment of eGene overlap
320 between the two stages to annotate GWAS loci. While GWAS loci that colocalized with fetal-adult shared e_gQTL
321 modules were more likely to modulate the expression of the same genes (75%; n = 24), ~25% displayed different
322 regulatory functions. Specifically, three loci were associated with partially overlapping eGenes (category C) and five
323 were associated with entirely different eGenes (category D and E) (Table S13). Similarly, for GWAS loci that
324 colocalized with fetal-adult shared e_{AS}QTL modules, 90% (9/10) were associated with splice changes of the same gene
325 (categories A and B) while 10% (1/10) was associated with at least one different gene between fetal-like and adult
326 (category C) (Table S13). These results show that while the function of shared GWAS regulatory variants is likely
327 conserved across fetal-like and adult pancreatic stages, a subset (21.4%, n = 9) are associated with distinct genes
328 between the two stages.

329 In total, we identified 397 GWAS loci (248 singleton and 149 module) colocalized with fetal-like and/or adult pancreas
330 eQTLs. To demonstrate the power of the pancreas eQTL resource that we have generated, below we describe how our
331 findings have contributed to biological insights in eight GWAS loci for pancreatic traits and diseases. Our examples
332 show that our study provides putative causal mechanisms and temporal context underlying genetic associations with
333 pancreatic complex traits and disease. We further demonstrate the regulatory plasticity of GWAS variants to produce
334 different transcriptional effects on gene expression between fetal-like and adult pancreas.

335 **Singleton e_gQTLs:** Here, we elucidate probable causal mechanisms for GWAS loci associated with FG levels and
336 T1D-risk that colocalized with iPSC-PPC-unique singleton e_gQTLs.

337 *chr8:80998464-81093464 and TPD52 (iPSC-PPC-unique singleton)*

338 We found that in the chr8:80998464-81093464 locus, a GWAS signal associated with FG levels colocalized with a
339 fetal-like iPSC-PPC-unique singleton e_gQTL for *TPD52*, also known as tumor protein D52 (effect size = -0.99, PP.H4
340 = 91.7%) (Figure 6A, Figure S14A, Table S13). The reported causal variant underlying this GWAS signal is

341 rs12541643²; however, colocalization with our eQTLs identified rs12549167 (chr8:81078464:C>T, PP = 33.9%, $r^2 =$
342 0.317 with rs12541643, Table S14) as the most likely candidate causal variant underlying both *TPD52* expression in
343 fetal-like iPSC-PPC and FG association. *TPD52* directly interacts with the AMP-activated protein kinase and
344 negatively affects AMPK signaling. AMPK controls a wide range of metabolic processes and is responsible for
345 maintaining cellular energy homeostasis particularly in tissues associated with obesity, insulin resistance, T2D, and
346 cancer such as muscle, liver, hypothalamus, and the pancreas⁵²⁻⁵⁵. Dysregulation of AMPK has also been associated
347 with developmental defects in which AMPK activation can lead to fetal malformation⁵⁶. Our findings suggest that
348 decreased expression of *TPD52* during development may influence changes in glucose metabolism and therefore
349 fasting glucose levels in adult.

350 *chr9:4232083-4352083 and CDC37L1-DT (iPSC-PPC-unique singleton)*

351 We found that the well-known *GLIS3* GWAS locus associated with FG and T1D-risk^{57,58} colocalized with a fetal-like
352 iPSC-PPC-unique singleton e_gQTL for the lncRNA *CDC37L1* divergent transcript (*CDC37L1-DT*; effect size = 1.46;
353 PP.H4 for FG and T1D = 92.4% and 91.2%, respectively, Figure 6B, Figure S14B, Table S13). Consistent with
354 previous studies^{57,58}, we identified rs10758593 (chr9:4292083:G>A, PP = 79.2%) as the lead candidate causal variant
355 underlying both eQTL and GWAS associations. Because *GLIS3* plays a critical role in pancreatic beta cell development
356 and function^{58,59,60}, it has often been reported as the susceptibility gene for this signal, however it remains unclear what
357 effects rs10758593 has on *GLIS3* expression. Our analysis suggests that another potential gene target of rs10758593
358 during pancreas development is *CDC37L1-DT*. While the molecular function of *CDC37L1-DT* is unknown, the gene
359 has been associated with 9p duplication in neurodevelopmental disorders⁶². Furthermore, a recent study observed a
360 significant association between the rs10758593 risk allele and birth weight, indicating a development role played by
361 this locus⁶³. Although additional studies are needed to understand the function of *CDC37L1-DT* during pancreas
362 development and in T1D pathology, our analysis indicates that *CDC37L1-DT* may be another candidate susceptibility
363 gene for the variants in the *GLIS3* locus. Assessment of *GLIS3* e_gQTLs in the three pancreatic tissues showed that that
364 is no overlap between the e_gQTLs and GWAS variants (Figure S15A).

365 **Combinatorial e_gQTLs:** Below, we describe two GWAS intervals associated cholesterol, LDL direct levels, and T1D.
366 We show that the GWAS variants colocalized with combinatorial e_gQTLs, indicating that multiple genes, and possibly
367 multiple developmental stages of the pancreas, may be involved in trait predisposition.

368 *chr22:41049522-41449522 and ADSL and STI3 (fetal-adult combinatorial)*

369 We found that the GWAS signals associated with cholesterol and LDL direct levels in the chr22:41049522-41449522
370 locus⁶⁴ colocalized with a “fetal-adult” e_gQTL module (module ID: GE_22_63, category E) (Figure 6C, Figure S14C-
371 D, Table S13). The module was associated with different eGenes between fetal-like iPSC-PPC and both adult
372 pancreatic tissues, in which the GWAS variants were associated with *ADSL* expression in iPSC-PPC (effect size =
373 0.78) but *STI3* expression in both adult pancreatic tissues (effect size = -0.15 in adult endocrine and 0.27 in adult
12

374 exocrine). Infants born with ADSL (adenylosuccinate lyase) deficiency suffer from impaired glucose and lipid
375 metabolism while ST13, also known as Hsc70-interacting protein, is involved in lipid metabolism⁶⁵. Overexpression
376 of *ST13* was found to result in disordered lipid metabolism in chronic pancreatitis⁶⁵. Although *ST13* was reported to
377 be the candidate causal gene for this locus⁶⁴, we determined that the underlying variants may also affect *ADSL*
378 expression but specifically during early pancreas development. Congruent with the previous study⁶⁴, our colocalization
379 identified rs138349 (chr22:41249522:A>G, PP = 21.9%) as the lead candidate causal variant for the e_gQTLs and both
380 cholesterol and LDL GWAS associations (Table S14). Altogether, annotation of the chr22:41049522-41449522
381 GWAS locus using our pancreatic eQTL resource suggests that altered expression of *ADSL* during pancreas
382 development and *ST13* in adult tissues may contribute to changes in cholesterol and LDL direct levels in adult.
383 Additional studies are required to understand the degree to which *ADSL* and *ST13* are causal for cholesterol and LDL
384 direct levels.

385 *chr10:90001035-90066035 and PTEN and LIPJ (adult exocrine-unique combinatorial)*

386 We found a T1D-risk signal in the chr10:90001035-90066035 locus that colocalized with an “adult exocrine-unique”
387 e_gQTL module (module ID: GE_10_35) associated with *PTEN* and *LIPJ* expression in adult pancreatic exocrine (effect
388 size = 0.48 and 0.49, respectively) (Figure S15B, Figure S14E, Table S13). Colocalization identified the distal
389 regulatory variant rs7068821 (chr10:90051035:G>T; PP = 85.5%) as the most likely candidate causal variant (Table
390 S14), which is in LD with the reported index SNP rs10509540 ($r^2 = 0.876$) in the GWAS catalogue. While *RNLS* was
391 reported to be the susceptibility gene for this locus⁶⁶, our analysis suggests that *PTEN* and *LIPJ* may be candidate
392 causal genes for this locus. Previous studies have shown that pancreas-specific *PTEN* knockout (PPKO) mice resulted
393 in enlarged pancreas and elevated proliferation of acinar cells. PPKO mice also exhibited hypoglycemia,
394 hypoinsulinemia, and altered amino metabolism⁶⁷. *LIPJ* encodes the lipase family member J and is involved in lipid
395 metabolism⁶⁸. Our findings provide additional biological insight into the chr10:900001035-90066035 T1D locus and
396 support previous studies suggesting a potential causal role of the adult exocrine pancreas in T1D pathogenesis^{3,63}.

397 **Singleton e_{AS}QTLs:** Here, we illustrate three examples of putative causal variants involved in alternative splicing in
398 the fetal-like pancreas. Long-noncoding RNAs (lncRNAs) have previously been shown to play important roles in
399 pancreatic diseases⁶⁹. Two of our examples include lncRNAs while one is a protein-coding gene.

400 *chr14:101286447-101326447 and MEG3 (iPSC-PPC-unique singleton)*

401 The chr14:101286447-101326447 is a well-known GWAS locus associated with T1D and has been reported to affect
402 the lncRNA maternally expressed gene 3 (*MEG3*). While the role of *MEG3* in T1D and T2D pathogenesis has been
403 extensively studied^{70–72}, the genetic mechanism by which this locus affects *MEG3* expression and therefore, T1D risk
404 is not well understood. Using our pancreatic eQTL resource, we found that the GWAS signal colocalized with a fetal-
405 like iPSC-PPC-unique singleton e_{AS}QTL for a *MEG3* isoform (ENST00000522618, PP.H4 = 98%, effect size = 1.3,
406 Figure 7A, Figure S16A, Table S13). Colocalization with the *MEG3* e_{AS}QTL identified rs56994090

407 (chr14:101306447:T>C, PP = 100%) as the most likely candidate causal variant, which is concordant with the findings
408 of a previous GWAS study ⁷³ (Table S14). Given that rs56994090 is located in the novel intron enhancer of *MEG3* ⁷⁴,
409 we hypothesize that alternative splicing of *MEG3* may alter the enhancer's regulatory function, as previously observed
410 in other lncRNAs ⁷⁴, and thereby, affect T1D-risk. Altogether, our findings describe a potential causal mechanism for
411 the T1D-risk locus involving differential alternative splicing of *MEG3* specifically during pancreas development.

412 *chr16:684685635-68855635 and CDH3 (iPSC-PPC-unique singleton)*

413 We determined a known GWAS signal in the chr16:684685635-68855635 locus associated with HbA1c levels ⁷⁵
414 colocalized with a fetal-like iPSC-PPC-unique singleton eQTL for the P-cadherin 3 (*CDH3*) isoform
415 ENST00000429102 (effect size = -1.6, PP.H4 = 83.1%) (Figure 7B, Figure S16B, Table S13). Colocalization using
416 the eASQTL identified intronic variant rs72785165 (chr16:68755635:T>A, PP = 6.8%) as the most likely candidate
417 causal variant (Table S14), which is in high LD with the reported GWAS SNP (rs4783565, $r^2 = 0.88$) ⁷⁵. While no
418 studies have examined how alternative splicing of *CDH3* affects HbA1c levels, studies have shown that chimeric
419 proteins made of cadherin ectodomains, including the P-cadherin CDH3, are important for proper insulin secretion by
420 pancreatic beta cells ⁷⁶. Based on our findings, we hypothesize that differential isoform usage of *CDH3* during pancreas
421 development may influence glucose control and therefore, HbA1c levels, in adults.

422 **Combinatorial eASQTLs:** Here, we present potential causal mechanisms during pancreas development that involve
423 alternative splicing and are associated with T2D-risk and BMI.

424 *chr13:30956642-31116642 and HMGB1 (iPSC-PPC-unique combinatorial)*

425 The GWAS signals associated with T2D and BMI in the chr13:30956642-31116642 locus ⁷⁷⁻⁸⁰ colocalized with the
426 iPSC-PPC-unique eASQTL module (module ID: AS_13_2) associated with three *HMGB1* isoforms:
427 ENST00000326004, ENST00000339872, and ENST00000399494 (effect size = 2.16, -0.85, and -2.26, respectively)
428 (Figure 7C, Figure S16C-E, Table S13). Our colocalization identified rs3742305 (chr13:31036642:C>G, PP = 49.3%)
429 as the lead candidate causal variant underlying this locus, in which the risk allele (G) was associated with increased
430 usage of ENST00000326004 and decreased usages of ENST00000339872 and ENST00000399494 (Figure S16C-E,
431 Table S6, Table S14). While a previous study ⁷⁹ also reported *HMGB1* as the susceptibility gene, the precise mechanism
432 by which rs3742305 affected *HMGB1* expression was unclear. HMGB1, also known as high-mobility group box 1, is
433 an important mediator for regulating gene expression during both developmental and adult stages of life. Deletion of
434 *HMGB1* disrupts cell growth and causes lethal hypoglycemia in mouse pups ⁸¹. In T2D, *HMGB1* promotes obesity-
435 induced adipose inflammation, insulin resistance, and islet dysfunction ⁸⁴. Our results suggest that differential usage of
436 *HMGB1* isoforms during pancreas development may affect adult risk of developing obesity and/or T2D.

437 Altogether, our findings demonstrate the value of our pancreatic eQTL resource to annotate GWAS risk variants with
438 fetal-like and adult temporal and regulatory information. We show that some causal regulatory variants underlying

439 disease-associated signals may influence adult traits by modulating the expression of genes in early development, while
440 in other cases, they may display regulatory plasticity and exert their effects by modulating the expression of multiple
441 different genes in fetal-like and adult pancreatic stages. Further, we identified an association between exocrine pancreas
442 and T1D, supporting a potential role of this tissue in diabetes pathogenesis³.

443 **Discussion**

444 In this study, we leveraged one of the most well-characterized iPSC cohorts comprising >100 genotyped individuals
445 to derive pancreatic progenitor cells and generate a comprehensive eQTL resource for examining genetic associations
446 with gene expression and isoform usage in fetal-like pancreatic cells. We discovered 8,665 eQTLs in the fetal-like
447 iPSC-PPCs and showed that 60% of eGenes were associated with regulatory variation specifically active during
448 pancreas development. For the eGenes that were shared with adult, ~12% were regulated by different genomic loci,
449 indicating that different regulatory elements modulate the same gene in fetal-like and adult pancreas. We further
450 identified regulatory variants that displayed developmental-specific function, 70% of which were uniquely active in
451 only iPSC-PPC while in other cases, the variants were active in both developmental and adult contexts but exhibited
452 regulatory plasticity in the genes they regulate. These results concur with previous studies showing that the genetic
453 regulatory landscape changes between fetal tissues and their adult counterparts^{41,43,83}, and therefore, highlights the
454 importance of assessing variant function in both fetal and adult tissue contexts. Furthermore, it is widely known that
455 tight regulation of genes during development is essential⁸⁴, and our study reflects this in our findings that the majority
456 of developmental-unique eQTLs were restricted to a single eGene. Because conditional associations were not readily
457 available for the adult pancreatic tissues, additional analyses are required to recapitulate our findings.

458 Finally, we highlighted examples of GWAS associations for which we utilized our temporally informed eQTL resource
459 to characterize novel causal risk mechanisms underlying adult pancreatic disease. We showed that some causal
460 regulatory variants underlying GWAS signals identified in the fetal-like iPSC-PPCs modulate the expression of genes
461 in early development, while others may exert their effects by modulating the expression of multiple different genes
462 across fetal-like and adult pancreatic stages. Of note, many of the fetal-unique regulatory variants underlying the
463 GWAS signals were eASQTLs, which is consistent with alternative splicing playing a key role in developing tissues<sup>49-
464 51,85</sup>. Hence, we believe that contribution of alternative splicing differences during fetal pancreas development to
465 complex traits warrants further investigation given the novel biology presented in our results.

466 We offer limitations in our study and potential future directions for the field at large. We believe that studies using
467 larger sample sizes are needed to identify additional associations between genetic variation and gene expression in fetal
468 samples. Our eQTL mapping in iPSC-PPC was conducted on much fewer samples compared to the other two studies
469 that used ~400 samples, rendering our dataset underpowered and not being able to capture weaker eQTL associations
470 that could be shared with the adult pancreatic tissues. Therefore, some of the eQTLs we annotated as adult endocrine-

471 unique or exocrine-unique may in reality be shared with fetal pancreas. On the other hand, the eQTLs we annotated as
472 iPSC-PPC-unique are less likely to be shared, as the signals in the adult datasets are better powered and therefore
473 sufficient for comparing against iPSC-PPC signals. Additionally, with the rapid generation of eQTL datasets from
474 different tissue contexts ^{1,2}, the development and application of artificial intelligence and machine learning as ways to
475 identify shared eQTL associations between multiple tissues will be extremely useful. While pairwise colocalization
476 and network analysis was able to identify shared eQTL regulatory loci across the fetal-like and two adult pancreatic
477 tissues in our study, machine learning approaches would enable these analyses to scale across spatiotemporal contexts
478 of all tissues and thereby, provide insights into regulatory elements that are unique to a specific context, as well as
479 those that display regulatory plasticity across multiple contexts.

480 In summary, our study provides a valuable resource for discovering causal regulatory mechanisms underlying
481 pancreatic traits and disease across developmental and adult timepoints of the pancreas. We revealed that disease
482 variants may either display temporal-specificity in which they affect gene expression specifically in one timepoint, or
483 regulatory plasticity, in which they affect gene expression in multiple timepoints but affect different genes. Our findings
484 lay the groundwork for future employment of development contexts for the characterization of disease-associated
485 variants.

486 **Methods**

487 **Subject Information**

488 We used iPSC lines from 106 individuals recruited as part of the iPSCORE project (Table S1). There were 53
489 individuals belonging to 19 families composed of two or more subjects (range: 2-6). Each subject was assigned an
490 iPSCORE_ID (i.e., iPSCORE 4_1), where “4” indicates the family number and “1” indicates the individual number,
491 and a 128-bit universal unique identifier (UUID). The 106 individuals included 68 females and 38 males with ages
492 ranging from 15 to 88 years old at the time of enrollment. Recruitment of these individuals was approved by the
493 Institutional Review Boards of the University of California, San Diego, and The Salk Institute (project no. 110776ZF).
494 Each of the subjects provided consent to publish information for this study.

495 **iPSC Generation**

496 Generation of the 106 iPSC lines has previously been described in detail ³⁰. Briefly, cultures of primary dermal
497 fibroblast cells were generated from a punch biopsy tissue ⁸⁷, infected with the Cytotune Sendai virus (Life
498 Technologies) per manufacturer’s protocol to initiate reprogramming. Emerging iPSC colonies were manually picked
499 after Day 21 and maintained on Matrigel (BD Corning) with mTeSR1 medium (Stem Cell Technologies). Multiple
500 independently established iPSC clones (i.e. referred to as lines) were derived from each individual. Many of the iPSC

501 lines were evaluated by flow cytometry for expression of two pluripotent markers: Tra-1-81 (Alexa Fluor 488 anti-
502 human, Biolegend) and SSEA-4 (PE anti-human, Biolegend)³⁰. Pluripotency was also examined using PluriTest-
503 RNaseq³⁰. This iPSCORE resource was established as part of the Next Generation Consortium of the National Heart,
504 Lung and Blood Institute and is available to researchers through the biorepository at WiCell Research Institute
505 (www.wicell.org; NHLBI Next Gen Collection). For-profit organizations can contact the corresponding author directly
506 to discuss line availability.

507 **Pancreatic Progenitor Differentiation**

508 We performed pancreatic progenitor cell (PPC) differentiation on each of the 106 iPSC lines. One iPSC line was
509 differentiated twice giving a total of 107 differentiations. Each differentiation was assigned a 128-bit universally unique
510 identifier (UUID), and a unique differentiation ID (UDID; “PPCXXX”), where “XXX” represents a numeric integer
511 (Table S2).

512 *Differentiation Protocol*

513 The iPSC lines were differentiated into PPCs using the STEMdiff™ Pancreatic Progenitor Kit (StemCell Technologies)
514 protocol with minor modifications. Briefly, iPSC lines were thawed into mTeSR1 medium containing 10 μM Y-27632
515 ROCK Inhibitor (Selleckchem) and plated onto one well of a 6-well plate coated with Matrigel. iPSCs were grown
516 until they reached 80% confluency⁸⁸ and then passaged using 2mg/ml solution of Dispase II (ThermoFisher Scientific)
517 onto three wells of a 6-well plate (ratio 1:3). To expand the iPSC cells for differentiation, iPSCs were passaged a second
518 time onto six wells of a 6-well plate (ratio 1:2). When the iPSCs reached 80% confluency, cells were dissociated into
519 single cells using Accutase (Innovative Cell Technologies Inc.) and resuspended at a concentration of 1.85×10^6
520 cells/ml in mTeSR medium containing 10 μM Y-27632 ROCK inhibitor. Cells were then plated onto six wells of a 6-
521 well plate and grown for approximately 16 to 20 hours to achieve a uniform monolayer of 90-95% confluence ($3.7 \times$
522 10^6 cells/well; about 3.9×10^5 cells/cm²). Differentiation of the iPSC monolayers was initiated by the addition of the
523 STEMdiff™ Stage Endoderm Basal medium supplemented with Supplement MR and Supplement CJ (2 ml/well) (Day
524 1, D1). The following media changes were performed every 24 hours following initiation of differentiation (2 ml/well).
525 On D2 and D3, the medium was changed to fresh STEMdiff™ Stage Endoderm Basal medium supplemented with
526 Supplement CJ. On D4, the medium was changed to STEMdiff™ Pancreatic Stage 2-4 Basal medium supplemented
527 with Supplement 2A and Supplement 2B. On D5 and D6, the medium was changed to STEMdiff™ Pancreatic Stage
528 2-4 Basal medium supplemented with Supplement 2B. From D7 to D9, the medium was changed to STEMdiff™
529 Pancreatic Stage 2-4 Basal medium supplemented with Supplement 3. From D10 to D14, the medium was changed to
530 STEMdiff™ Pancreatic Stage 2-4 Basal medium supplemented with Supplement 4. On D15, cells were dissociated
531 with Accutase and then collected, counted, and processed for data generation. iPSC-PPC cells were cryopreserved in
532 CryoStor® CS10 (StemCell Technologies).

533 *iPSC-PPC Differentiation Efficiency*

534 To evaluate the efficiency of iPSC-PPC differentiation, we performed flow cytometry on two pancreatic precursor
535 markers, PDX1 and NKX6-1. Specifically, at least 2×10^6 cells were fixed and permeabilized using the
536 Fixation/Permeabilized Solution Kit with BD GolgiStop™ (BD Biosciences) following the manufacturer's
537 recommendations. Cells were resuspended in 1x BD Perm/Wash™ Buffer at a concentration of 1×10^7 cells/ml. For
538 each flow cytometry staining, 2.5×10^5 cells were stained for 75 minutes at room temperature with PE Mouse anti-
539 PDX1 Clone-658A5 (BD Biosciences; 1:10) and Alexa Fluor® 647 Mouse anti-NKX6.1 Clone R11-560 (BD
540 Bioscience; 1:10), or with the appropriate class control antibodies: PE Mouse anti-IgG1 κ R-PE Clone MOPC-21 (BD
541 Biosciences) and Alexa Fluor® 647 Mouse anti IgG1 κ Isotype Clone MOPC-21 (BD Biosciences). Stained cells were
542 washed three times, resuspended in PBS containing 1% BSA and 1% formaldehyde, and immediately analyzed using
543 FACS Canto II flow cytometer (BD Biosciences). The fraction of PDX1- and NKX6-1-positive was calculated using
544 FlowJo software version 10.4 (Table S2).

545 **WGS data**

546 Whole-genome sequencing data for the 106 iPSCORE individuals were downloaded from dbGaP (phs001325) as a
547 VCF file²⁹. We retained variants with MAF > 5% across all 273 individuals in the iPSCORE resource, that were in
548 Hardy-Weinberg equilibrium ($p > 10^{-6}$), and that were within 500 Kb of the expressed gene's body coordinates.
549 Specifically, we expanded the coordinates of each of the 16,464 expressed autosomal genes (500 Kb upstream and
550 downstream) and extracted all variants within these regions using *bcftools view* with parameters *--fPASS -q 0.05:minor*
551⁸⁹. Next, we normalized indels and split multi-allelic variants using *bcftools norm -m-* and removed variants that were
552 genotyped in fewer than 99% of samples using *bcftools filter -i 'F_PASS(GT!="mis") > 0.99*⁸⁹. Finally, we converted
553 the resulting VCF files to text using *bcftools query*⁸⁹ and converted the genotypes from character strings (0/0, 0/1, and
554 1/1) to numeric (0, 0.5, and 1, respectively). This resulted in 6,593,484 total variants used for eQTL mapping.

555 **Bulk RNA-seq**

556 *Library Preparation and Sequencing*

557 RNA was isolated from total-cell lysates using the Quick-RNA™ MiniPrep Kit (Zymo Research) with on-column
558 DNase treatments. RNA was eluted in 48 μ l RNase-free water and analyzed on a TapeStation (Agilent) to determine
559 sample integrity. All iPSC-PPC samples had RNA integrity number (RIN) values over 9. Illumina TruSeq Stranded
560 mRNA libraries were prepared according to the manufacturer's instructions and sequenced on NovaSeq6000 for 101bp
561 paired-end sequencing.

562 *Data Processing and Quality Control*

563 FASTQ files were obtained for all 107 iPSC-PPC samples and processed using a similar pipeline described in our
564 previous studies^{29,90}. Specifically, RNA-seq reads were aligned with STAR (2.7.3)⁹¹ to the hg19 reference using
565 GENCODE version 34 hg19⁹² splice junctions with default alignment parameters and the following adjustments: -
566 *outFilterMultimapNmax 20*, *-outFilterMismatchNmax 999*, *-alignIntronMin 20*, *-alignIntronMax 1000000*, -
567 *alignMatesGapMax 1000000*. BAM files were sorted by coordinates, and duplicate reads were marked using Samtools
568 (1.9.0)⁸⁹. RNA-seq QC metrics were calculated using Samtools (1.9.0) *flagstat*⁸⁹, Samtools (1.9.0) *idxstats*⁸⁹, and
569 Picard (2.20.1) *CollectRnaSeqMetrics*⁹³. Across all 107 iPSC-PPC samples, the total read depth ranged from 32.3 M
570 to 160.4 M (mean = 70.7), the median percentage of intergenic bases was 3.31%, the median percentage of mRNA
571 bases was 92.1%, and the median percentage of duplicate reads was 22.2% (Table S2).

572 *Sample Identity*

573 We obtained common bi-allelic variants from the 1000 Genomes Phase 3 panel⁹⁴ with minor allele frequencies between
574 45% and 55% and predicted their genotypes in the 107 bulk RNA-seq samples using *mpileup* and *call* functions in
575 BCFtools (1.9.0)^{95,96}. Then, we used the *genome* command in plink⁹³ to estimate the identity-by-state (IBS) between
576 each pair of bulk RNA-seq and WGS samples. All RNA-seq samples were correctly matched to the subject with
577 *PI_HAT* > 0.95 (Table S2).

578 *Quantification of gene expression and relative isoform usage*

579 We calculated TPM and estimated relative isoform usage for each gene in each RNA-seq sample using RSEM (version
580 1.2.20)⁹⁷ with the following options *-seed 3272015 -estimate-rspd -paired-end -forward-prob*. To identify expressed
581 autosomal genes and isoforms to use for eQTL analyses, we used the same approach previously described¹². Briefly,
582 autosomal genes were considered expressed if $TPM \geq 1$ in at least 10% of samples. To identify expressed isoforms,
583 we required that isoforms had $TPM \geq 1$ and usage $\geq 10\%$ in at least 10% of samples and corresponded to expressed
584 genes with at least two expressed isoforms. In total, 16,464 autosomal genes were used for e_gQTL analysis, and 29,871
585 autosomal isoforms corresponding to 9,624 genes were used for e_iQTL analysis. We quantile-normalized TPM and
586 isoform usage across all 107 samples using the *normalize.quantiles* (preprocessCore) and *qnorm* functions in R (version
587 4.2.1) to obtain a mean expression = 0 and standard deviation = 1.

588 *Inferring pseudotime using Monocle*

589 We obtained FASTQ files for 213 iPSCs^{29,30} (phs000924), 176 adult pancreatic exocrine⁸ (phs000424), and
590 87 adult pancreatic endocrine³¹ (GSE50398), and processed the data using the same pipeline described above
591 to obtain TPM counts for each gene per sample. We then used Monocle (<http://cole-trapnell-lab.github.io/monocle-release/docs/#constructing-single-cell-trajectories>)⁹⁸ to infer the pseudotime on all of

593 the RNA-seq samples, including the 107 iPSC-PPCs. Following the standard workflow under “Constructing Single
594 Cell Trajectories” in the Monocle tutorial, we provided TPM counts for all overlapping autosomal expressed genes in
595 the four tissues as input. Then, we identified differentially expressed genes using *differentialGeneTest*, ordered them
596 (*setOrderingFilter*), and performed dimension reduction analysis using *reduceDimension* with *max_components* = 2
597 and *method* = “*DDRTree*”. Pseudotime was calculated by rooting time (pseudotime = 0) in the 213 iPSC-PPCs using
598 the *GM_state* and *orderCells* functions provided in the tutorial (Table S5).

599 *PCA analysis with iPSCs, adult pancreatic exocrine, and adult pancreatic endocrine*

600 We obtained TPM counts (described above) for the 213 iPSCs²⁹, 176 adult exocrine⁸, 87 adult endocrine³¹, and the
601 107 iPSC-PPCs and performed PCA analysis on the 2,000 most variable genes across the samples using *prcomp* in R
602 (version 4.2.1) with *scale* = *T* and *center* = *T*. We observed that the PC clusters corresponded to the iPSCs and each
603 of the three pancreatic tissue types: iPSC-PPC, adult endocrine, and adult exocrine (Figure S9, Table S5).

604 **scRNA-seq**

605 To characterize the cellular composition of the fetal-like iPSC-PPC samples, we performed single-cell RNA-seq
606 (scRNA-seq) on one iPSC line (from differentiation PPC034) and ten iPSC-PPC samples with varying percentages of
607 double-positive PDX1+/NKX6-1+ cells based on flow cytometry (range: 9.4-91.7%) (Figure S2, Figure S3, Table S2).
608 Because bulk RNA-seq was generated on cryopreserved cells, we sought to also examine whether cell cryopreservation
609 affects gene expression estimates using scRNA-seq. Therefore, we included both freshly prepared (i.e., not frozen and
610 processed immediately after differentiation) and cryopreserved cells for four iPSC-PPC samples (PPC029, PPC027,
611 PPC023, PPC034; Table S2) for scRNA-seq processing.

612 *Sample Collection*

613 Fresh cells from the iPSC line and seven iPSC-PPC samples were captured individually at D15. Cells from four of
614 these same iPSC-PPC samples that had been cryopreserved were pooled and captured immediately after thawing
615 (RNA_Pool_1). Cells from an additional three iPSC-PPC samples were captured only after cryopreservation
616 (RNA_Pool_2) (Table S2).

617 *Library Preparation and Sequencing*

618 All single cells were captured using the 10X Chromium controller (10X Genomics) according to the manufacturer’s
619 specifications and manual (Manual CG000183, Rev A). Cells from each scRNA-seq sample (one iPSC, seven fresh
620 iPSC-PPCs, RNA_Pool_1, and RNA_Pool_2) were loaded each onto an individual lane of a Chromium Single Cell
621 Chip B. Libraries were generated using Chromium Single Cell 3’ Library Gel Bead Kit v3 (10X Genomics) following
622 manufacturer’s manual with small modifications. Specifically, the purified cDNA was eluted in 24 µl of Buffer EB,

623 half of which was used for the subsequent step of the library construction. cDNA was amplified for 10 cycles and
624 libraries were amplified for 8 cycles. All libraries were sequenced on a HiSeq 4000 using custom programs (fresh: 28-
625 8-175 Pair End and cryopreserved: 28-8-98 Pair End). Specifically, eight libraries generated from fresh samples (one
626 iPSC and seven iPSC-PPC samples) were pooled together and loaded evenly onto eight lanes and sequenced to an
627 average depth of 163 million reads. The two libraries from seven cryopreserved lines (RNA_Pool_1 and RNA_Pool_2)
628 were each sequenced on an individual lane to an average depth of 265 million reads. In total, we captured 99,819 cells.
629 We observed highly correlated cell type proportions between fresh and cryopreserved iPSC-PPC samples (Figure S8).

630 *scRNA-seq Alignment*

631 We obtained FASTQ files for the ten scRNA-seq samples (one iPSC, seven fresh iPSC-PPCs, RNA_Pool_1, and
632 RNA_Pool_2) (Table S2) and used CellRanger V6.0.1 (<https://support.10xgenomics.com/>) with default parameters
633 and GENCODE version 34 hg19⁹² gene annotations to generate single-cell gene counts and BAM files for each of the
634 ten samples.

635 *Dataset Integration and Quality Control*

636 We processed the single-cell gene counts by first aggregating the iPSC and seven fresh iPSC-PPC samples using the
637 *aggr* function on CellRanger V6.0.1 with *normalization = F*. Then, we integrated the aggregated dataset (“aggr”) with
638 the two pools of cryopreserved samples (RNA_Pool_1 and RNA_Pool_2) using the standard integration workflow
639 described in Seurat (version 3.2; <https://satijalab.org/seurat/archive/v3.2/integration.html>). Specifically, for each
640 dataset (aggr, RNA_Pool_1, and RNA_Pool_2), we log-normalized the gene counts using *NormalizeData* (default
641 parameters) then used *FindVariableFeatures* with *selection.method = “vst”*, *nfeatures = 2000*, and *dispersion.cutoff*
642 *= c(0.5, Inf)* to identify the top 2,000 most variable genes in each dataset. We then used *FindIntegrationAnchors* and
643 *IntegrateData* with *dims = 1:30* to integrate the three datasets. We scaled the integrated data with *ScaleData*, performed
644 principal component analysis with *RunPCA* for *npcs = 30*, and processed for UMAP visualization (*RunUMAP* with
645 *reduction = “pca”* and *dims = 1:30*). Clusters were identified using *FindClusters* with default parameters.

646 To remove low-quality cells, we examined the distribution of the number of genes per cell and the percentage of reads
647 mapping to the mitochondrial chromosome (chrM) in each cluster. We removed the cluster (11,677 cells) with fewer
648 than 500 genes per cell and more than 50% of the reads mapping to chrM. We re-processed the filtered data (*ScaleData*,
649 *RunPCA*, *FindClusters*, *RunUMAP*) and removed a second cluster of cells that had the lowest median number of
650 expressed genes (723 versus 2,775) and highest median fraction of mitochondrial reads (34.0% versus 8.39%). After
651 this second filtering step, we retained 84,258 cells.

652 *Demultiplexing Sample Identity*

653 We used Demuxlet⁹⁹ to assign pooled cryopreserved cells in RNA_Pool_1 and RNA_Pool_2 (19,136 cells in total) to
654 the correct iPSC-PPC sample. Specifically, we provided CellRanger Bam files and a VCF file containing genotypes
655 for biallelic SNVs located at UTR and exon regions on autosomes as annotated by GENCODE version 34 hg19⁹². We
656 excluded 33 cells that were incorrectly assigned to samples not associated with the pooled sample (i.e., cells from
657 RNA_POOL_1 were predicted to be from other samples not in RNA_Pool_1). 84,225 cells remained for downstream
658 analyses (Table S3).

659 *Annotation of Cell Type Clusters*

660 We annotated the scRNA-seq clusters by first clustering at three different resolutions (0.5, 0.08, and 0.1) (Figure S4-
661 6). We selected resolution = 0.08 because it best captured the expected iPSC-PPC cell types based on each cluster's
662 expression for the following gene markers: *POU5F1* (iPSC), *COL1A1*, *COL1A2* (mesendoderm) *AFP*, *APOA* (early
663 definitive endoderm), *GATA4*, *GATA6*, *PDX1* (early PPC), *PDX1*, *NKX6-1* (late PPC), *PAX6*, *CHGA*, *INS*, *GCG*, *SST*
664 (endocrine), and *FLT1* (early ductal). We validated our annotations by comparing the iPSC-PPC clusters to those
665 identified from scRNA-seq of ESC-PPC samples over 4 different stages of differentiation¹⁰⁰ (GSE114412): Stage 3
666 (Day 6; 7,982 cells), Stage 4 (Day 13; 6,960 cells), Stage 5 (Day 18; 4,193 cells), and Stage 6 (Day 25; 5,186 cells).
667 Specifically, we compared the expression patterns of the gene markers between the clusters using z-normalized mean
668 expression computed on cells expressing at least 1% of maximal expression for the gene, as described in the reference
669 study¹⁰⁰. Metadata containing single cell annotations are reported in Table S3.

670 *Differentially Expressed Genes*

671 To identify differentially expressed genes for each iPSC-PPC cluster, we used the *FindAllMarkers* function in Seurat
672¹⁰¹ with *logfc.threshold* = 0.01 and *min.pct* = 0.01. P-values were automatically adjusted using Bonferroni correction,
673 and genes with adjusted p-values ≤ 0.05 were considered differentially expressed (Table S4).

674 **eQTL Analysis**

675 To investigate the effects of genetic variation on gene expression in iPSC-PPCs, we performed an expression
676 quantitative trait loci (eQTL) analysis on gene expression and isoform usage. The eQTLs associated with gene
677 expression were defined as e_g QTLs while those associated with relative isoform usage were defined as e_i QTLs.

678 *Covariates for eQTL Mapping*

679 We included the following as covariates for eQTL mapping of both gene expression and isoform usage: 1) sex; 2)
680 normalized number of RNA-seq reads; 3) percent of reads that mapped to autosome or sex chromosomes (labeled as
681 “pct_uniquely_mapped_to_canonical_chromosomes” in Table S2); 4) percent of reads mapped to mitochondrial
682 chromosome; 5) 20 genotype principal components to account for global ancestry; 6) 20 PEER factors to account for

683 transcriptome variability; and 7) kinship matrix to account for genetic relatedness between samples. All covariates are
684 available in Table S1-3.

685 Genotype Principal Component Analysis (PCA): Global ancestry was estimated using the genotypes of the 439,461
686 common variants with minor allele frequency (MAF) between 45 and 55% in the 1000 Genomes Phase 3 Panel⁹⁴. We
687 merged the VCF files for the 106 iPSCORE subjects and the 2,504 subjects in the 1000 Genomes⁹⁴ and performed a
688 PCA analysis using *plink --pca*⁹³ (Figure S1A). The top 20 principal components were used as covariates in the eQTL
689 model to account for global ancestry and can be found in Table S1.

690 PEER Factors: We sought to determine the optimal number of PEER factors to use in the eQTL analysis that will result
691 in maximal eGene discovery. To this end, we initially calculated PEER factors on the 10,000 expressed genes with the
692 largest variance across all samples. To limit biases due to the expression levels of each gene, we divided the 16,464
693 expressed genes into ten deciles based on their average TPM, and selected 50 genes from each decile, for a total of 500
694 genes. We next performed eQTL analysis on each of the 500 genes using 10 to 60 PEER factors in increments of 10.
695 While 30 PEER factors resulted in the highest percentage of eGenes (14.0%), we opted for using 20 PEER factors
696 because the eQTL analysis had a comparable percentage of eGenes (11.8%) to GTEx tissues with similar sample sizes
697¹⁰ (Figure S18). Although we observed variable fraction of double-positive PDX1+/NKX6-1+ cells in the iPSC-PPC
698 samples, we did not include this variable as a covariate because PEER factors 1 and 4 already accounted for this
699 variability (Figure S19).

700 Kinship Matrix: The kinship matrix was included as a random effects term to account for the genetic relatedness
701 between individuals in our cohort. We constructed the kinship matrix using the same 439,461 variants employed above
702 using the *-make-rel square* function in *plink*⁹³. The kinship matrix is available in Table S2.

703 *eQTL Analysis*

704 We performed eQTL analysis using the same method described in our previous study¹². For each expressed autosomal
705 gene and isoform, we tested variants that were within 500 Kb of the gene body coordinates using the *bcftools query*
706 function. To account for the genetic relatedness between the samples, we performed eQTL mapping using a linear
707 mixed model with the *scan* function in *limix* v.3.0.4¹⁰² that incorporates the kinship matrix as a random effects term.
708 Specifically, eQTL mapping was implemented through the following model:

$$709 \quad y_i = \beta_{ji} \cdot g_j + \sum_{n=1}^N \beta_n \cdot C_n + u + \epsilon_{ij}$$

710 Where y_i is the normalized expression value for gene i , β_{ji} is the effect size of genotype of SNP j on gene i , g_j is the
711 genotype of SNP j , β_n is the effect size of covariate n , C_n is a vector of values for covariate n , u is the kinship matrix
712 as a random effect, and ϵ is the error term for the association between expression of gene i and genotype of SNP j . As

713 described above, we used the following as covariates: 1) sex, 2) normalized number of RNA-seq reads, 3) percent of
714 reads mapped to autosomal or sex chromosome, 4) percent of reads mapped to mitochondrial chromosome, 5) the top
715 20 genotype PCs (to account to global ancestry), and 6) the top 20 PEER factors (to account for confounders of
716 expression variability), and are available in Tables S1-2.

717 *FDR Correction*

718 To perform FDR correction, we used a two-step procedure described in Huang et al.¹⁰³, which first corrects at the
719 gene level and then at the genome-wide level. First, we performed FDR correction on the p-values of all variants tested
720 for each gene or isoform using eigenMT¹⁰², which considers the LD structure of the variants. Then, we extracted the
721 lead eQTL for each gene or isoform based on the most significant FDR-corrected p-value. If more than one variant had
722 the same FDR-corrected p-value, we selected the one with the largest absolute effect size as the lead eQTL. For the
723 second correction, we performed an FDR-correction on all lead variants using the Benjamini-Hochberg method (q-
724 value) and considered only eQTLs with q-value ≤ 0.01 as significant (Table S6).

725 *Conditional eQTLs*

726 To identify additional independent eQTLs (i.e., conditional eQTLs) for each eGene and eIsoform, we performed a step-
727 wise regression analysis in which the genotype of the lead eQTL was included as a covariate in the model and the
728 eQTL mapping procedure (regression and multiple test correction) was re-performed. We repeated this analysis to
729 discover up to five additional associations for each eGene and eIsoform. Conditional eQTLs with q-values ≤ 0.01 were
730 considered significant (Table S6).

731 **Functional characterization of iPSC-PPC eQTLs**

732 *Fine-mapping of eQTL Associations*

733 To define a credible set of candidate causal variants for each eQTL association, we performed genetic fine-mapping
734 using the *finemap.abf* function in *coloc* (version 5.1.0, R)³⁵. This Bayesian method converts p-values of all variants
735 tested for a specific gene to posterior probabilities (PP) of association for being the causal variant. Variants with PP \geq
736 1% are available in Table S7. The eQTLs not present in this table do not having any variants with PP $\geq 1\%$ (i.e., all
737 variants were estimated to have PP $< 1\%$).

738 *Genomic enrichments of e_g QTLs and e_i QTLs*

739 For each independent eQTL association, we obtained candidate causal variants whose PP $\geq 5\%$ (Table S7) and
740 determined their overlap with each of the following genomic annotations using *bedtools intersect*: short splice acceptor
741 sites (± 50 bp), long splice acceptor sites (± 100 bp), splice donor sites (± 50 bp), UTR, intron, exon, intergenic,
742 promoters, and RNA-binding protein binding sites (RBP-BS). RBP-BS were downloaded from a published dataset that

743 utilized enhanced CLIP to identify binding sites of 73 RBPs¹⁰⁴. We considered only binding sites with irreproducible
744 discovery rate (IDR) threshold of 0.01, indicating that these sites were reproducible across multiple biological samples.
745 Enrichment of candidate causal variants for genomic regions was calculated using a Fisher's Exact Test comparing the
746 proportion of SNPs that overlap each annotation between e_gQTLs and e_iQTLs. P-values were corrected using the
747 Benjamini-Hochberg method and were considered significant if their FDR-corrected p-value ≤ 0.05 (Figure 1E).

748 *Quantification of allele-specific binding of transcription factors using GVATdb*

749 To annotate each candidate causal variant by their effects on transcription factor (TF) binding, we used the Genetic
750 Variants Allelic TF Binding Database (GVATdb) to estimate the TF binding impact score associated with each variant
751 and each of the 58 iPSC-PPC-expressed TF available on the database and with a AUPRC > 0.75 indicating a high-
752 confidence deltaSVM model. We estimated the score using the instructions and reference files provided on the
753 GVATdb GitHub repository (<https://github.com/ren-lab/deltaSVM>). The software required a list of SNPs as input
754 along with hg19 reference files provided in the GVATdb repository. The output provides the deltaSVM score¹⁰⁵ for
755 each variant-TF pair (Table S8), indicating whether the variant results in a promotion ("Gain"), disruption ("Loss"), or
756 no change ("None") in TF binding.

757 *Correlation between eQTL effect size and binding affinity of transcription factors*

758 To determine whether e_gQTLs were more likely to affect TF binding compared to e_iQTLs, we performed a Spearman
759 Correlation Analysis between deltaSVM score and eQTL effect size on candidate causal variants with PP $\geq 10\%$, 20%,
760 40%, 60% and 80%. We considered nominal p-value ≤ 0.05 as significant.

761 *Colocalization between iPSC-PPC gene and isoform eQTLs*

762 To determine the overlap of genetic variants between e_gQTLs and e_iQTLs for the same gene, we performed Bayesian
763 colocalization using the *coloc.abf* function in *coloc* (version 5.1.0, R)³⁵, where each pair of signals was given a
764 summary PP that each of the following five hypotheses was true: H0) no association was detected in both signals, H1)
765 an association was detected in signal 1, H2) an association was detected in signal 2, H3) an association was detected
766 in both signals but the underlying causal variants are different, and H4) an association was detected for both signals
767 and the underlying causal variants are the same. We considered two eQTL signals to be shared if the number of
768 overlapping variants used to test for colocalization (called "nsnps" in *coloc.abf* output) ≥ 500 and the PP for H4 (called
769 "PP.H4.abf" in *coloc.abf* output; hereafter referred to as PP.H4) $\geq 80\%$. Conversely, two signals were considered
770 distinct if nsnps ≥ 500 and PP for H3 (called "PP.H3.abf" in *coloc.abf* output; hereafter referred to as PP.H3) $\geq 80\%$.
771 eQTL associations with PP.H4 $< 80\%$ and PP.H3 $< 80\%$ were due to insufficient power in one or both eQTL signals.
772 As input into *coloc.abf*, we provided p-values, minor allele frequency, and sample size. All associations with PP $\geq 80\%$
773 for any model are available in Table S9.

774 Genomic enrichment of overlapping e_g QTL and e_i QTL signals compared to non-overlapping

775 To test the enrichment of overlapping e_g QTLs and e_i QTLs in genomic regions compared to non-overlapping signals,
776 we used a similar approach described in a previous study¹⁰. We determined the overlap of candidate causal variants
777 with $PP \geq 1\%$ in each genomic annotation using *bedtools intersect* and compared the proportion of variants overlapping
778 each annotation against a background set of 20,000 random variants using a Fisher's Exact Test. For overlapping
779 e QTLs, we used the candidate causal variants predicted in the *coloc.abf* output. Enrichments with nominal p-value <
780 0.05 were considered significant (Figure S10).

781 Downloading eQTL summary statistics for adult pancreatic tissues

782 We downloaded complete eQTL summary statistics for gene and exon associations for 420 adult pancreatic endocrine
783 from the InSPIRE Consortium (<https://zenodo.org/record/3408356>)¹¹, and gene and splicing associations for 305 adult
784 pancreatic exocrine from the GTEx Data Portal for GTEx Analysis version 8¹⁰
785 (<https://console.cloud.google.com/storage/browser/gtex-resources>). All GTEx SNPs were converted to hg19 using the
786 UCSC liftOver Bioconductor package in R (<https://www.bioconductor.org/help/workflows/liftOver/>). Complete
787 statistics for conditional associations in the adult endocrine and exocrine datasets were not readily available and
788 therefore, not included in our analyses.

789 Due to the different types of eQTLs used in this study, we hereafter refer to all eQTLs as a collective unit as “eQTLs”,
790 eQTLs that are associated with gene expression as “ e_g QTLs”, and eQTLs associated with changes in alternative splicing
791 (e_i QTLs, exon eQTLs, and sQTLs) as “ e_{AS} QTLs”.

792 Comparing eGenes between iPSC-PPC and adult endocrine

793 To identify eGenes that were shared between iPSC-PPC and adult pancreatic endocrine tissues, we compared the 4,065
794 eGenes in iPSC-PPC and the 4,211 eGenes in adult endocrine that complete summary statistics were available for.
795 Specifically, we used the *intersect* function in R to identify eGenes that overlapped between the two tissues and *setdiff*
796 function in R to identify eGenes that did not overlap. Similarly, using the *intersect* function in R, we compared the
797 22,266 expressed genes in adult endocrine tissues with the 4,065 eGenes in iPSC-PPC to identify the proportion of
798 iPSC-PPC eGenes that were expressed in adult endocrine, and vice versa with the 17,098 expressed genes in iPSC-
799 PPC and 4,211 eGenes in adult endocrine. The 22,266 expressed genes in adult endocrine tissues were obtained from
800 the complete summary statistics uploaded by the previous study in <https://zenodo.org/record/3408356>.

801 Comparing eQTLs present in fetal-like iPSC-PPC and adult pancreatic tissues

802 *Colocalization between iPSC-PPC and adult eQTLs*

803 To identify eQTLs whose effects were driven by the same causal signals in iPSC-PPC and adult pancreatic tissues
804 (endocrine and exocrine), we performed Bayesian colocalization using the *coloc.abf* function in *coloc* (version 5.1.0,
805 R)³⁵. Specifically, for each iPSC-PPC and adult eQTL, we tested its overlap with nearby eQTLs within 3 Mb from the
806 gene body coordinates. eQTLs with no overlapping variants would automatically not be tested. Then, we filtered the
807 results by requiring that each colocalization used the number of overlapping variants (called “nsnps” in the *coloc.abf*
808 output) ≥ 500 . As described above, we considered two eQTL signals to be shared if PP.H4 $\geq 80\%$ or distinct if PP.H3
809 $\geq 80\%$. eQTL associations with PP.H4 $< 80\%$ and PP.H3 $< 80\%$ were due to insufficient power in one or both eQTL
810 signals.

811 Because we, and others, have shown that e_g QTLs are functionally different from e_{AS} QTLs (e_g QTLs, exon eQTLs, and
812 splicing eQTLs), we performed colocalization for e_g QTLs and e_{AS} QTLs independently (i.e., colocalization of e_g QTL
813 was performed only with another e_g QTL and an e_{AS} QTL only with another e_{AS} QTL). All associations with PP $\geq 80\%$
814 for any model are reported in Table S9.

815 *Fine-mapping of adult eQTL associations*

816 Similarly for iPSC-PPC eQTLs, we identified candidate causal variants using the *finemap.abf* function in *coloc* (version
817 5.1.0, R). This Bayesian method converts p-values of all variants tested for a specific gene to a PP value for being the
818 causal variant. Variants with PP $\geq 1\%$ are available in Table S7. The eQTLs not present in this table do not having any
819 variants with PP $\geq 1\%$ (i.e., all variants were estimated to have PP $< 1\%$).

820 **For all downstream analyses beyond this point, we used only iPSC-PPC, adult pancreatic endocrine, and adult**
821 **pancreatic exocrine eQTLs with at least one candidate causal variant with PP $\geq 1\%$, outside of the MHC region,**
822 **and are annotated in GENCODE version 34 hg19, to ensure that our analyses were powered sufficiently and the**
823 **multiple datasets were comparable.**

824 *Identifying tissue-unique singleton eQTLs*

825 Singleton eQTLs were defined in this study as an eQTL not colocalizing or in LD ($r^2 \geq 0.2$ and within 500 Kb) with
826 another eQTL in the same or different pancreatic tissue. Singleton eQTLs were also considered tissue-unique as they
827 were functional in only the tested tissue. For each eQTL that did not display a H4 association with another eQTL, we
828 examined their LD with nearby eQTLs of the same phenotype (gene expression or alternative splicing) in all three
829 pancreatic tissues using their most likely candidate causal variants based on the highest PP (from *finemap.abf* output).
830 LD was calculated using *plink --r2 square --keep-allele-order --make-bed*⁹³ and the 1000 Genomes Phase 3 panel⁹⁴.
831 A singleton eQTL was considered in LD with another eQTL if the singleton’s candidate causal variant was within 500
832 Kb and in LD ($r^2 \geq 0.2$) with another eQTL’s candidate causal variant. If the candidate causal variant was not genotyped

833 in the 1000 Genomes Phase 3 panel, then we used the next top candidate causal variant and repeat the process, if
834 needed, until no more variant was remaining with causal PP \geq 1%. If none of the candidate causal variants with PP \geq
835 1% were genotyped in 1000 Genomes, then we used distance as a metric for determining potential associations, where
836 if the singleton candidate causal variant was within 500 Kb with another eQTL's candidate causal variant, we
837 considered them to be potentially associated. A singleton eQTL in LD or potentially associated based on distance was
838 annotated as “ambiguous” and excluded from further analysis, otherwise we annotated the eQTL as a tissue-unique
839 singleton. All annotated tissue-unique singleton eQTLs are reported in Table S10.

840 *Identifying eQTL modules*

841 eQTL modules were identified by first creating a network using the *graph_from_data_frame* function in igraph
842 (version 1.3.4, R) ¹⁰⁶ where the input was a data frame containing all pairs of colocalized eQTLs (nsnps \geq 500 and
843 PP.H4 \geq 80%) as binary edges. We created networks for each chromosome and phenotype (gene expression and
844 alternatively splicing) independently, totaling to 44 networks (22 chromosomes x 2 phenotypes = 44 networks). Then,
845 we performed community detection analysis using the *cluster_leiden* function with *--objective_function* =
846 “modularity”, *n_iterations* = 500, *resolution* = 0.3 to identify modules of eQTLs. Upon examining them in depth, we
847 observed that 5% of the modules contained at least one H3 association (PP.H3 \geq 80%) between a pair of eQTLs,
848 indicating that signals within a module were predicted to have distinct genetic variants despite being assigned to the
849 same module. Therefore, to filter for modules that contained eQTLs likely to share the same genetic variants, we
850 required that at least 30% of all eQTL pairs had a H4 association and that the number of H4 “edges” was twice the
851 number of H3 “edges” (number of H4 edges / number of H3 edges \geq 2). For example, a module with four eQTLs would
852 have six possible pairwise combinations, and to be considered a validated module, we required at least two H4 edges
853 and no more than one H3 edge. Modules that did not pass these thresholds were annotated as “module_failed” and
854 excluded from downstream analyses. Summary of eQTL modules and their individual eQTL associations are reported
855 in Table S11. Module IDs were assigned such that the first term indicates the phenotype the module was associated
856 with (“GE” for gene expression or “AS” for alternative splicing), the second term indicates the chromosome number,
857 and the third term indicates a unique integer. For example, “GE_1_32” indicates that this module is associated with
858 changes in gene expression, located in in chromosome 1, and assigned the number 32.

859 *Identifying tissue-unique and tissue-sharing eQTL modules*

860 Combinatorial eQTLs were defined in this study as an eQTL having at least one H4 association (PP.H4 \geq 80%) with
861 another eQTL either in the same or different tissue. These combinatorial eQTLs then connect to form a module, which
862 we identified using the network analysis described above. We then categorized each module based on the activity of
863 eQTLs in the three pancreatic tissues, having a total of seven module categories:

864 1) Fetal-unique: contains eQTLs in **only** iPSC-PPC

- 865 2) Adult endocrine-unique: contains eQTLs in **only** adult endocrine
- 866 3) Adult exocrine-unique: contains eQTLs in **only** adult exocrine
- 867 4) Adult-shared: contains eQTLs in adult endocrine **and** adult exocrine
- 868 5) Fetal-endocrine: contains eQTLs in iPSC-PPC **and** adult endocrine
- 869 6) Fetal-exocrine: contains eQTLs in iPSC-PPC **and** adult exocrine
- 870 7) Fetal-adult: contains eQTLs in **all** three pancreatic tissues

871 We next filtered the eQTL modules based on their LD relationships with other tissues to confirm the module's tissue
872 specificity. For example, we required fetal-endocrine modules to contain eQTLs specific to only iPSC-PPC and adult
873 endocrine and not be in LD with an eQTL from adult exocrine. Similar to the analysis described above for identifying
874 tissue-unique singletons, we calculated LD between each pair of eQTLs' most likely candidate causal variants (based
875 on the highest PP; $PP \geq 1\%$) using *plink --r2 square --keep-allele-order --make-bed*⁹³ and the 1000 Genomes Phase 3
876 panel⁹⁴. For each of the module categories, we required that the following were true to be considered for downstream
877 analyses:

- 878 1) Fetal-unique: contains eQTLs in only iPSC-PPC, and **all** eQTLs were not in LD with eQTLs in adult
879 endocrine **and** adult exocrine
- 880 2) Adult endocrine-unique: contains eQTLs in only adult endocrine, and **all** eQTLs were not in LD with
881 eQTLs in adult exocrine **and** iPSC-PPC
- 882 3) Adult exocrine-unique: contains eQTLs in only adult exocrine, and **all** eQTLs were not in LD with
883 eQTLs in adult endocrine **and** iPSC-PPC
- 884 4) Adult-shared: contains eQTLs in only adult endocrine and adult exocrine, and **all** eQTLs were not in
885 LD with eQTLs in iPSC-PPC
- 886 5) Fetal-endocrine: contains eQTLs in iPSC-PPC and adult endocrine, and **all** eQTLs were not in LD
887 with eQTLs in adult exocrine
- 888 6) Fetal-exocrine: contains eQTLs in iPSC-PPC and adult exocrine, and **all** eQTLs were not in LD with
889 eQTLs in adult endocrine
- 890 7) Fetal-adult: contains eQTLs in **all** three pancreatic tissues.

891 For any module that did not meet the above requirements, we annotated the eQTLs in the module "ambiguous" and
892 excluded for downstream analysis. Hereafter, we refer the eQTL associations in tissue-unique modules (categories 1-
893 3) as tissue-unique combinatorial eQTLs and those in categories 5-7 as eQTLs shared between both fetal-like and adult
894 stages. All annotations for eQTL modules and their individual eQTLs are reported in Table S10 and Table S11.

895 **Enrichment of tissue-unique eQTLs in pancreatic chromatin states**

896 We obtained chromatin state maps for adult endocrine and human embryonic stem cell-derived pancreatic progenitor
897 cells from previously published studies ^{21,107} and adult pancreatic exocrine from the Roadmap Epigenome Project
898 (epigenome ID: E098) ⁷. Because e_gQTLs were likely to affect non-coding regulatory elements (Figure 1E), we
899 examined their enrichments in chromatin states to better understand, and validate, their functional mechanisms.
900 Enrichments were calculated using a Fisher's Exact Test by comparing the proportion of candidate causal variants
901 (from *finemap.abf*, see above sections; PP ≥ 10%) of tissue-unique singleton and combinatorial e_gQTLs in each
902 chromatin state to a background set of 20,000 randomly selected variants. Enrichments with Benjamini-Hochberg-
903 corrected p-values ≤ 0.05 were considered significant. Enrichment results are available in Table S12, Figure 3I, and
904 Figure S11C. Functional plasticity of eQTLs in fetal-like and adult pancreatic tissues

905 For the modules shared between both fetal-like and adult pancreatic tissue (categories 5-7; described above), we
906 compared the eGenes associated with 1) iPSC-PPC eQTLs versus adult endocrine eQTLs and 2) iPSC-PPC eQTLs
907 versus adult exocrine eQTLs. For e_{AS}QTLs, we compared the genes mapping to 1) each isoform in iPSC-PPC versus
908 exon in adult endocrine and 2) each isoform in iPSC-PPC versus splice interval in adult exocrine. From these
909 comparisons, we assign each module an “endocrine_egene_overlap” label and an “exocrine_egene_overlap” label in
910 Table S11 (also shown in Figure 4A and Figure S12D), where “zero” indicates that the module does not contain an
911 eQTL in the adult tissue, “same” indicates that the module contains eQTLs associated with the same gene in iPSC-
912 PPC and adult, “partial” indicates that the module contains eQTLs associated with partially overlapping genes between
913 iPSC-PPC and adult, and “different” indicates that the module contains eQTLs associated with entirely different genes.
914 For example, if a module was annotated with “zero” for endocrine_egene_overlap and “same” for
915 exocrine_egene_overlap, this indicates that the module was shared between only fetal-like and adult exocrine (i.e.,
916 “fetal-exocrine” or category 6 as described above; does not contain an adult endocrine eQTL) and the genes associated
917 with this locus were the same in both tissues.

918 **Complex Trait GWAS Associations**

919 *Colocalization of eQTLs with GWAS associations*

920 We obtained GWAS summary statistics from ten different studies: 1) type 1 diabetes ³, 2) type 2 diabetes ¹⁰⁷, 3) body
921 mass index ⁴⁶, 4) triglycerides ⁴⁶, 5) HDL cholesterol ⁴⁶, 6) LDL direct ⁴⁶, 7) cholesterol ⁴⁶, 8) glycosylated hemoglobin
922 A1C (HbA1c) levels from the MAGIC Consortium ¹⁰⁸, 9) HbA1c levels from the Pan-UKBB Study ⁴⁶, and 10) fasting
923 glucose ¹⁰⁸. All of the data, except for type 1 diabetes, were provided in hg19 coordinates, therefore we converted the
924 coordinates from hg38 to hg19 using the liftOver package in R ¹⁰⁹. We sorted and indexed each file using *tabix* ⁸⁹. For
925 each trait, we performed colocalization between GWAS variants and all filtered significant eQTLs (see bolded section
926 above) in the three pancreatic tissues with the *coloc.abf* function in *coloc* (version 5.1.0, R) ³⁵ using p-values, MAF,
927 and sample size as inputs. Then, we filtered results based on whether the lead candidate causal variant underlying both
928 GWAS and eQTL association (from *coloc.abf* output) is genome-wide significant for GWAS association (p-value ≤

929 5×10^{-8}) and the number of overlapping variants used to test for colocalization ($n_{snps} \geq 500$). eQTLs were considered
930 to share a genetic signal with GWAS if $PP.H4 \geq 80\%$ or have distinct signals with GWAS if $PP.H3 \geq 80\%$. For eQTL
931 modules, we required that at least 30% of the eQTLs in the module colocalized with GWAS ($PP.H4 \geq 80\%$) and that
932 the number of H4 associations is twice the number of H3 associations (number of H4 associations / number of H3
933 associations ≥ 2). Colocalization results for the 397 GWAS loci with $PP.H4 \geq 80\%$ are available in Table S13.

934 *GWAS 99% Credible Sets*

935 For each GWAS locus (based on GWAS locus ID in Table S13), we constructed 99% credible sets with the predicted
936 candidate causal variants underlying both eQTL and GWAS associations (from *coloc.abf* output). If the GWAS locus
937 colocalized with a singleton eQTL, the credible sets were constructed using the output of the eQTL's colocalization
938 with GWAS. If the GWAS locus colocalized with an eQTL module, we constructed credible sets for each of the
939 pairwise eQTL-GWAS colocalization and retained the eQTL that resulted in the least number of candidate causal
940 variants. If multiple eQTLs had the same number of variants in their credible set, we considered the eQTL with the
941 highest $PP.H4$ for GWAS colocalization. 99% credible sets were constructed by first sorting the variants by descending
942 order of causal PP and obtaining the least number of variants that resulted in a cumulative $PP \geq 99\%$. 99% credible
943 sets for each of the 397 GWAS loci (248 singleton and 149 module) are reported in Table S14.

944 **Data Availability**

945 FASTQ sequencing data for iPSC-PPC scRNA-seq and bulk RNA-seq have been deposited into GSE152610 and
946 GSE182758, respectively. RNA-seq for iPSC, adult endocrine, and adult exocrine samples used in PCA and
947 pseudotime analyses were downloaded from phs000924, GSE50398, and phs000424, respectively. eQTL summary
948 statistics for adult endocrine and exocrine samples were obtained from the GTEx Data Repository
949 (<https://console.cloud.google.com/storage/browser/gtex-resources>) and a previously published study¹¹
950 (<https://zenodo.org/record/3408356>), respectively. WGS data for iPSCORE subjects were downloaded as a VCF file
951 from phs001325. GWAS summary statistics were obtained from the Pan UK BioBank resource
952 (<https://pan.ukbb.broadinstitute.org/>), the MAGIC (Meta-Analyses of Glucose and Insulin-related traits) Consortium
953 (<https://magicinvestigators.org/downloads/>; <https://doi.org/10.1038/s41588-021-00852-9>), the DIAMANTE
954 Consortium (<https://diagram-consortium.org/downloads.html>; <http://doi.org/10.1038/s41588-018-0241-6>), and a
955 previously published study³. Full eQTL summary statistics for iPSC-PPC, supplemental tables, and processed scRNA-
956 seq data have been deposited in Figshare: [https://figshare.com/projects/Large-scale_eQTL_analysis_of_iPSC-
957 PPC/156987](https://figshare.com/projects/Large-scale_eQTL_analysis_of_iPSC-PPC/156987).

958 **Author information**

959 **iPSCORE Consortium, University of California, San Diego, La Jolla, CA, 92093, US**

960 Angelo D. Arias, Timothy D. Arthur, Paola Benaglio, Victor Borja, Megan Cook, Matteo D’Antonio, Agnieszka
961 D’Antonio-Chronowska, Christopher DeBoever, Margaret K.R. Donovan, KathyJean Farnam, Kelly A. Frazer, Kyohei
962 Fujita, Melvin Garcia, Olivier Harismendy, David Jakubosky, Kristen Jepsen, Isaac Joshua, He Li, Hiroko Matsui,
963 Naoki Nariai, Jennifer P. Nguyen, Daniel T. O’Connor, Jonathan Okubo, Fengwen Rao, Joaquin Reyna, Lana Ribeiro
964 Aguiar, Bianca Salgado, Nayara Silva, Erin N. Smith, Josh Sohmer, Shawn Yost, William W. Young Greenwald

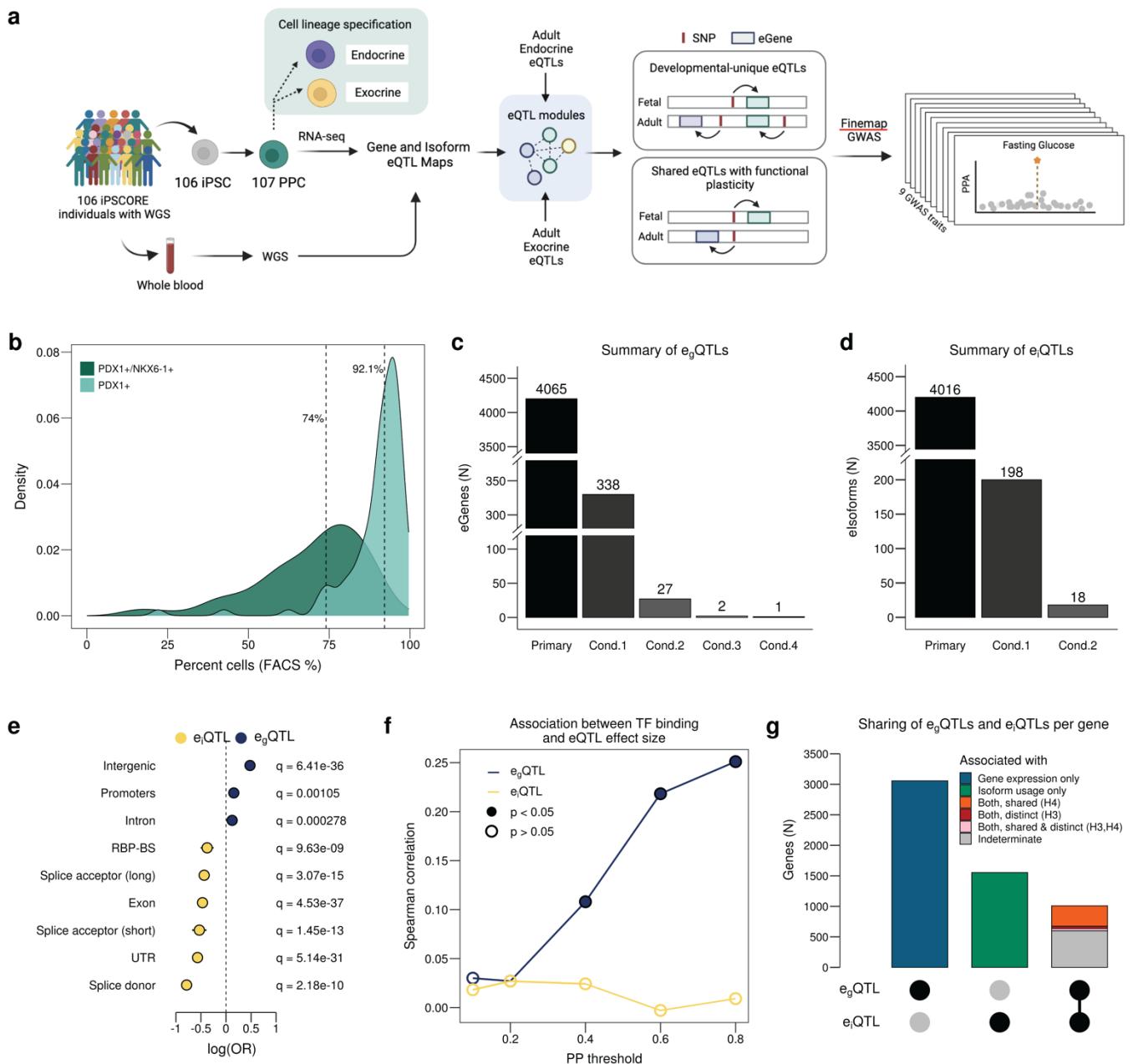
965 **Contributions**

966 KAF conceived the study. ADC, BS, and KF performed the differentiations and generated molecular data. JPN, MKRD
967 and HM performed quality check on scRNA-seq and RNA-seq samples. JPN and TDA performed the computational
968 analyses. KAF, ADC, MD oversaw the study. JPN, MD and KAF prepared the manuscript.

969 **Acknowledgements**

970 This work was supported by the National Library Training Grant T15LM011271 and the National Institute of Diabetes
971 and Digestive and Kidney Disease (NIDDK) F31DK131867, U01DK105541, DP3DK112155 and P30DK063491.
972 Additional support was also received from the National Heart, Lung and Blood Institute (NHLBI) F31HL158198. This
973 publication includes data generated at the UC San Diego IGM Genomics Center utilizing an Illumina NovaSeq 6000
974 that was purchased with funding from a National Institutes of Health SIG grant S10OD026929.

975 **Figure 1. Discovery and Characterization of eQTLs in iPSC-PPC**



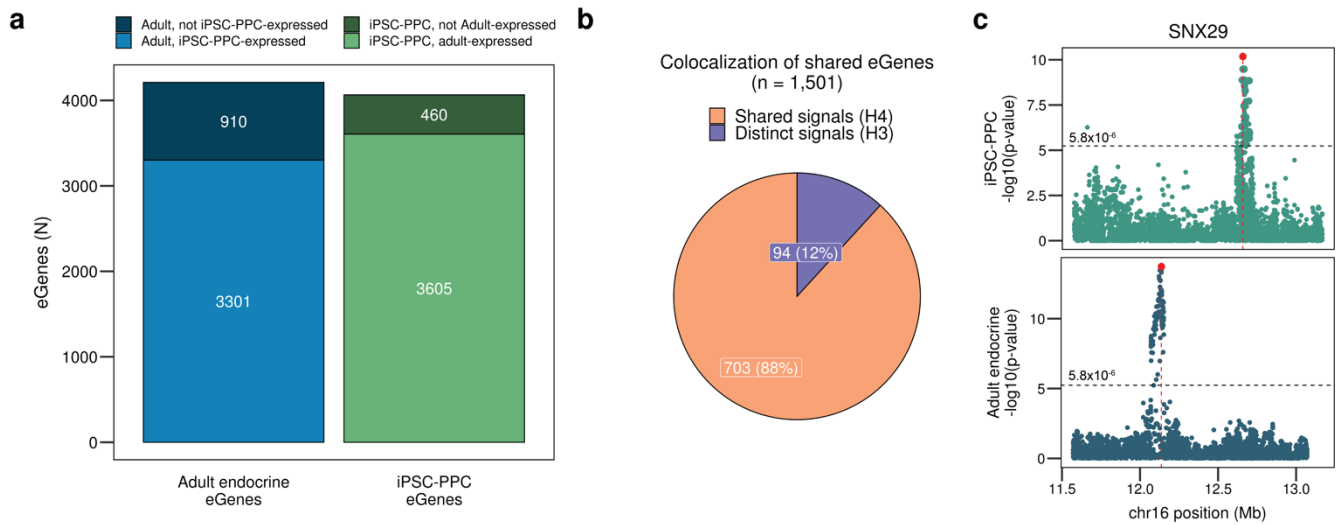
976

977 (a) Study overview. (b) Density plots showing the distribution of PDX1⁺ cells (%; regardless of NKX6-1 status; light
 978 green) and PDX1⁺/NKX6-1⁺ cells (%; dark green). (c) Bar plot showing the number of eGenes with primary and
 979 conditional e_g QTLs. (d) Bar plot showing the number of eIsoforms with primary and conditional eQTLs. (e)
 980 Enrichment (odds ratio) of eQTLs for functional genomic annotations using a two-sided Fisher's Exact Test comparing
 981 the proportion of SNPs with causal PP $\geq 5\%$ between e_g QTLs (blue; n = 8,763) and e_i QTLs (yellow; n = 8,919). (f)
 982 Line plot comparing the spearman correlation between TF binding score and eQTL effect size at different thresholds
 983 of PP for e_g QTLs (blue) and e_i QTLs (yellow). Closed points indicate significance of correlation based on nominal $p <$

33

984 0.05. (g) Bar plot showing the number of genes that have only e_g QTLs (blue; $n = 3,057$), only e_i QTLs (green; $n =$
985 1,554), or both. Orange represents genes with only overlapping e_g QTLs and e_i QTLs ($PP.H4 \geq 80\%$; $n = 333$) based on
986 colocalization. Red represents genes with only distinct e_g QTLs and e_i QTLs ($PP.H3 \geq 80\%$; $n = 38$), and pink represents
987 genes with both shared and distinct e_g QTLs and e_i QTLs (i.e., an eGene with two eIsoforms may colocalize with one
988 eIsoform but not the other) ($n = 39$). Gray represents genes whose eQTL signals were not sufficiently powered to test
989 for colocalization ($PP.H4 < 80\%$ and $PP.H3 < 80\%$; $n = 598$).

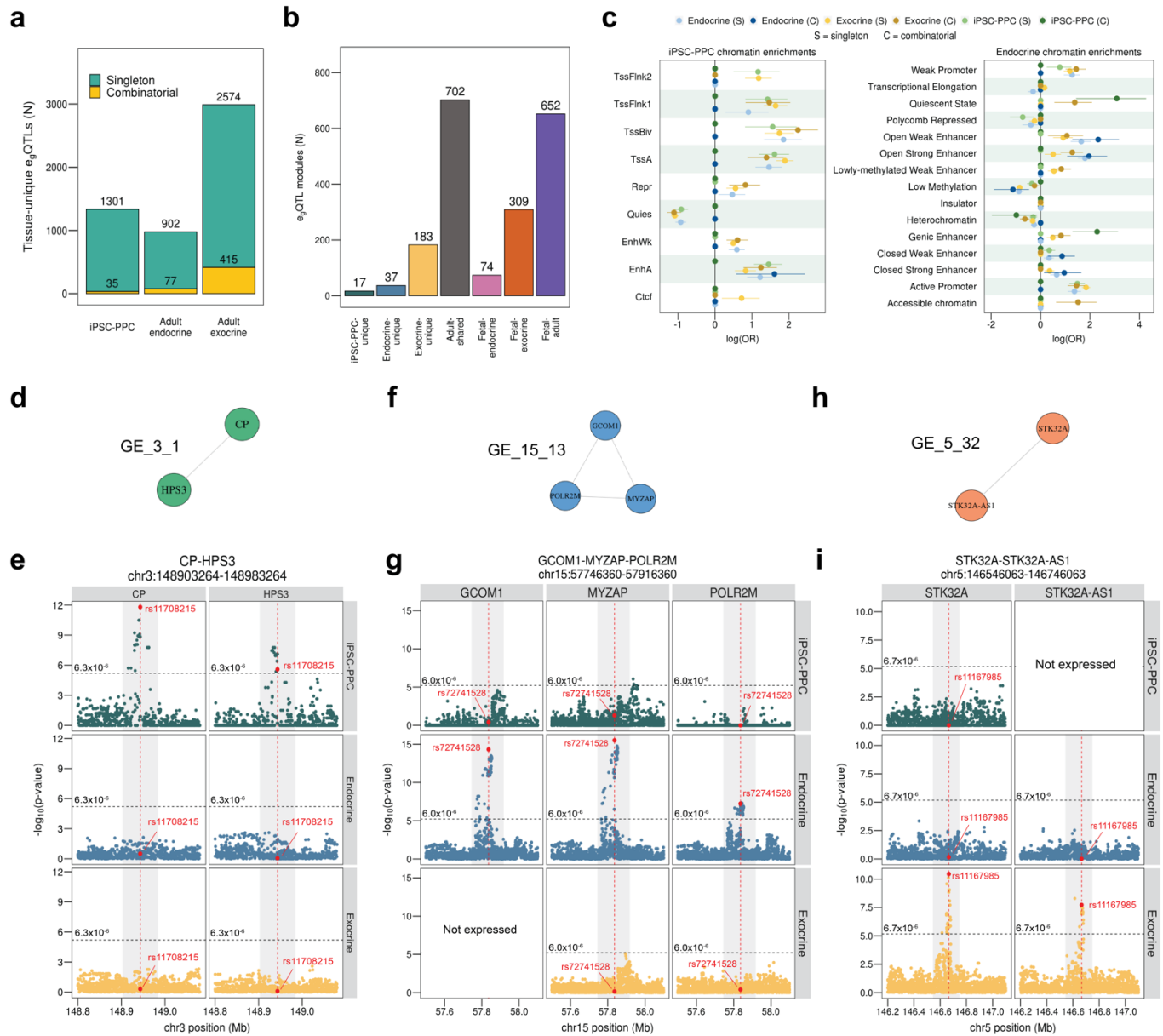
990 **Figure 2. Comparison of the genetic architecture underlying gene expression between**
991 **fetal-like and adult endocrine**



992

993 (a) Stacked bar plot showing the number of eGenes detected in adult endocrine (blue; $n = 4,211$ total) that are expressed
994 in iPSC-PPC. Likewise, we show the number of iPSC-PPC eGenes (green; $n = 4,065$ total) that are expressed in adult
995 endocrine. Darker shades represent eGenes that are expressed in the other tissue while lighter shades represent those
996 that were expressed. These results show that the majority of iPSC-PPC and adult endocrine eGenes were expressed in
997 the other tissue. Therefore, the small overlap of eGenes between the two tissues were not due to expression differences
998 but instead due to differences in the genetic regulatory landscape. (b) Pie chart showing that 12% of the shared eGenes
999 between iPSC-PPC and adult endocrine were associated with distinct genetic loci ($\text{PP.H3} \geq 80\%$), indicating that
1000 different regulatory mechanisms facilitate the expression of the same gene in iPSC-PPC and adult endocrine. (c)
1001 Example of a shared eGene (*SNX29*) whose expression was associated with different e_g QTL signals in iPSC-PPC
1002 (green, top panel) and adult endocrine (blue, bottom panel). For plotting purposes, we assigned a single p-value for
1003 gene-level significance based on Bonferroni-correction (0.05 divided by the number of variants tested for the gene;
1004 horizontal line). Red vertical lines indicate the positions of the lead variants in the adult endocrine and fetal-like iPSC-
1005 PPC based on p-value (chr16:12656135 and chr16:12136526, respectively).

Figure 3. eQTL sharing between iPSC-PPC and adult pancreas

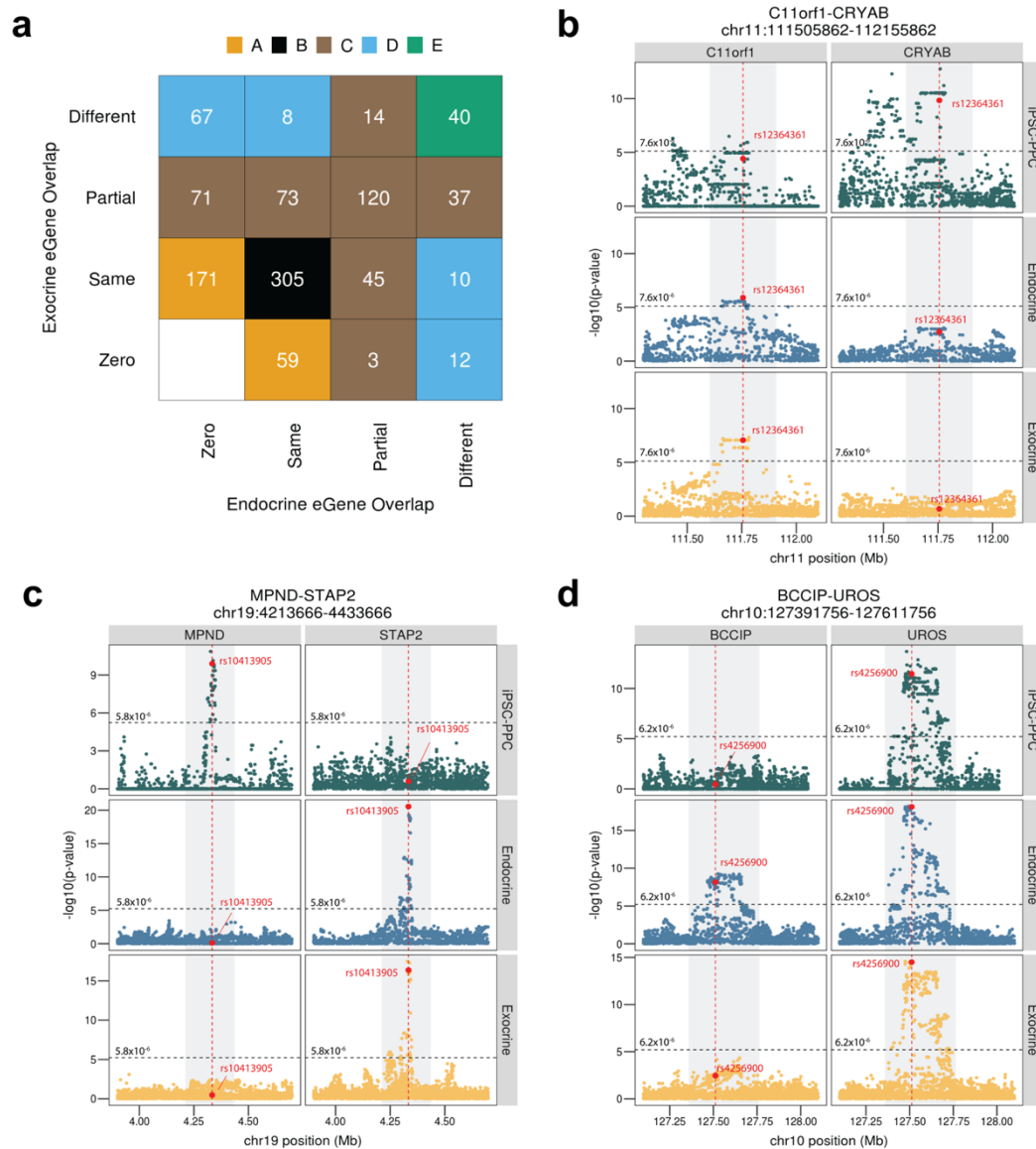


1008 (a) Bar plot showing the number of tissue-unique e_gQTLs identified in fetal-like iPSC-PPC, adult pancreatic endocrine,
 1009 and adult pancreatic exocrine. (b) Bar plot showing the number of e_gQTL modules for each annotation. (c) Plot showing
 1010 the enrichment (odds ratio) of tissue-unique singleton (S) and combinatorial (C) e_gQTLs in PPC²¹ (left) and endocrine
 1011⁴⁵ (right) chromatin states. Nomenclature for the chromatin states used in the previously studies was maintained.
 1012 Enrichment was tested using a two-sided Fisher's Exact Test comparing the proportion of candidate causal variants
 1013 with causal PP ≥ 20% overlapping the chromatin states between the e_gQTLs in question versus a background of
 1014 randomly selected 20,000 variants. P-values were Benjamini-Hochberg-corrected and considered significant if the
 1015 corrected p-values < 0.05. Non-significant results are set to log(odds ratio) = 0. Error bars represent 95% confidence

1016 intervals for the odds ratios. **(d-e)** The chr3:148903264-148983264 locus (gray rectangle) was an example of an “iPSC-
1017 PPC-unique” e_gQTL locus (module ID: GE_3_1) associated with *CP* and *HPS3* expression. **(f-g)** The chr15:57746360-
1018 57916360 locus (gray rectangle) was an example of an “adult endocrine-unique” e_gQTL locus (module ID: GE_15_13)
1019 associated with *GCOM1*, *MYZAP*, and *POLR2M* expression. We show that the e_gQTL locus was unique to adult
1020 endocrine and not active in iPSC-PPC and adult exocrine. *GCOM1* was not expressed in adult exocrine and therefore,
1021 was not tested for e_gQTL discovery. **(h-i)** The chr5:146546063-146746063 locus (gray box) is an example of an “adult
1022 exocrine-unique” e_gQTL locus (module ID: GE_5_32) associated with *STK32A* and *STK32A-ASI* expression only in
1023 adult endocrine. *STK32A-ASI* was not expressed in iPSC-PPC and therefore, was not tested for e_gQTL discovery. Panel
1024 **d, f, h** display the e_gQTL modules as networks in which the e_gQTL associations (nodes) are connected by edges based
1025 on colocalization (PP.H4 ≥ 80%). For plotting purposes, we assigned a single p-value for gene-level significance based
1026 on Bonferroni-correction (0.05 divided by the number of variants tested for the gene; horizontal line). Red vertical
1027 lines indicate the positions of the lead candidate causal variants underlying the colocalization based on maximum PP.

1028

Figure 4. Regulatory plasticity of e_g QTL loci

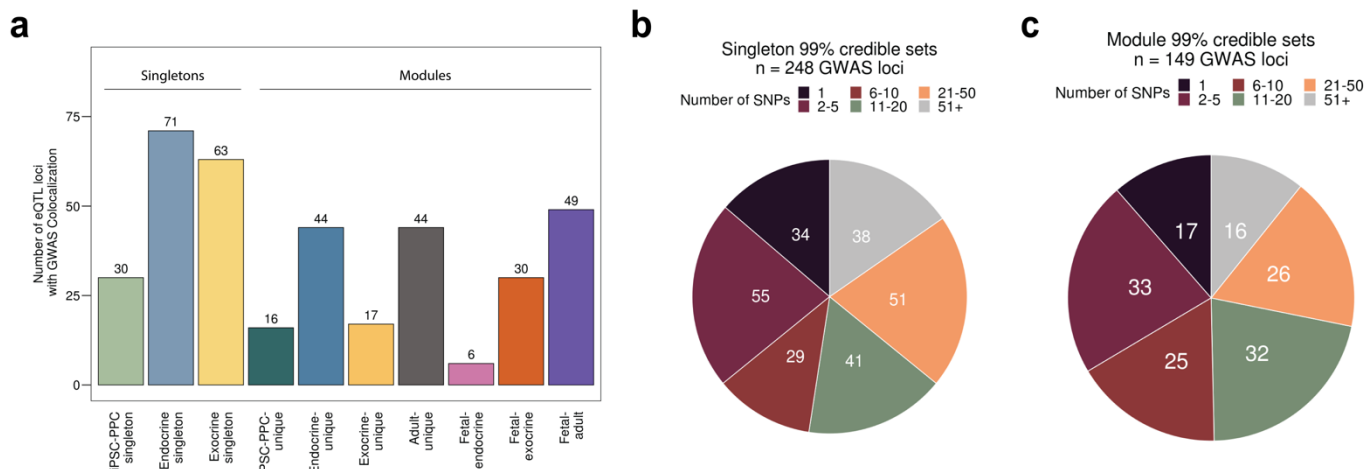


1029

1030 (a) Number of e_g QTL modules based on eGene overlap between iPSC-PPC and the two adult pancreatic tissues. “Zero”
 1031 indicates that the module does not contain an e_g QTL in the respective adult tissue. “Same” indicates that the module
 1032 contains e_g QTLs for only the same eGenes in iPSC-PPC and the adult tissue. “Partial” indicates that the module
 1033 contains e_g QTLs for partially overlapping eGenes between iPSC-PPC and the adult tissue. “Different” indicates that
 1034 the module contains e_g QTLs for only different eGenes between iPSC-PPC and the adult tissue. For example, the 171
 1035 e_g QTL modules in category A (orange) contain e_g QTLs from only iPSC-PPC and adult exocrine (zero e_g QTLs from
 1036 adult endocrine) and are associated with the same eGenes between the two tissues. (b-d) Examples of e_g QTL loci
 1037 demonstrating regulatory plasticity of genetic variation across fetal-like and adult pancreatic stages. Panel b shows a
 1038 locus associated with different eGenes in iPSC-PPC (*CRYAB*) and both the adult tissues (*C11orf1*). Panel c shows a

1039 locus associated with *MPND* expression in only iPSC-PPC but *STAP2* expression in both the adult tissues. Panel **d**
1040 shows a locus associated with partially overlapping eGenes between the two pancreatic stages (*UROS* in all three
1041 pancreatic tissues and *BCCIP* in only adult endocrine). For plotting purposes, we assigned a single p-value for gene-
1042 level significance based on Bonferroni-correction (0.05 divided by the number of variants tested for the gene; horizontal
1043 line). Red vertical lines indicate the positions of the lead candidate causal variants underlying the colocalization based
1044 on maximum PP.

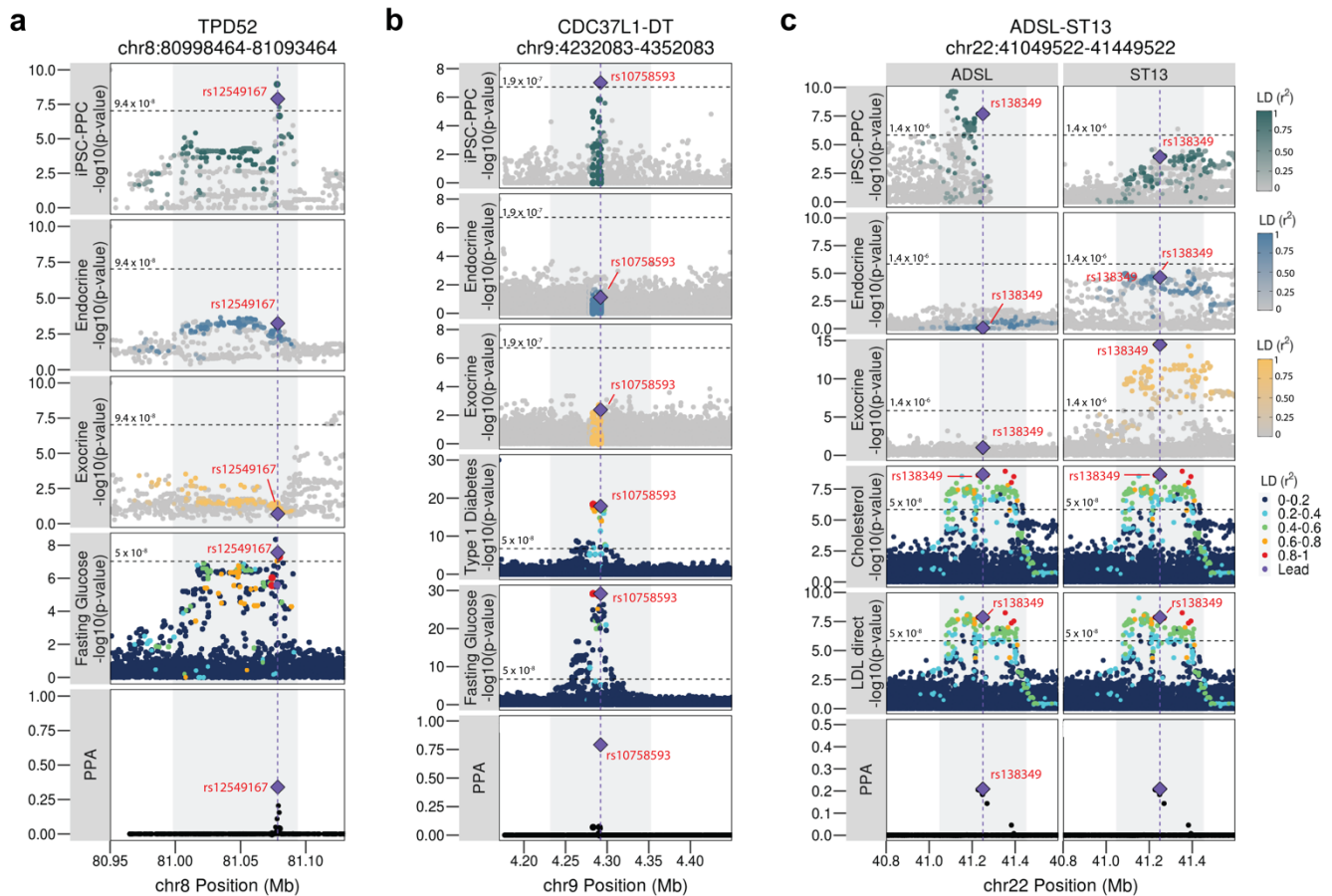
1045 **Figure 5. Summary of Pancreatic GWAS Associations**



1046

1047 (a) Bar plot showing the number of eQTL loci that colocalized with GWAS variants (PP.H4 ≥ 80%) as a singleton or
 1048 module. (b) Pie chart showing the number of singleton-colocalized GWAS loci (n = 248) color-coded by the number
 1049 of candidate causal variants identified in their 99% credible sets. (c) Pie chart showing the number of module-
 1050 colocalized GWAS loci (n = 149) color-coded by the number of candidate causal variants identified in their 99%
 1051 credible sets.

1052 **Figure 6. Pancreatic GWAS Associations with Fetal-specific and Adult-shared Gene**
 1053 **Expression**

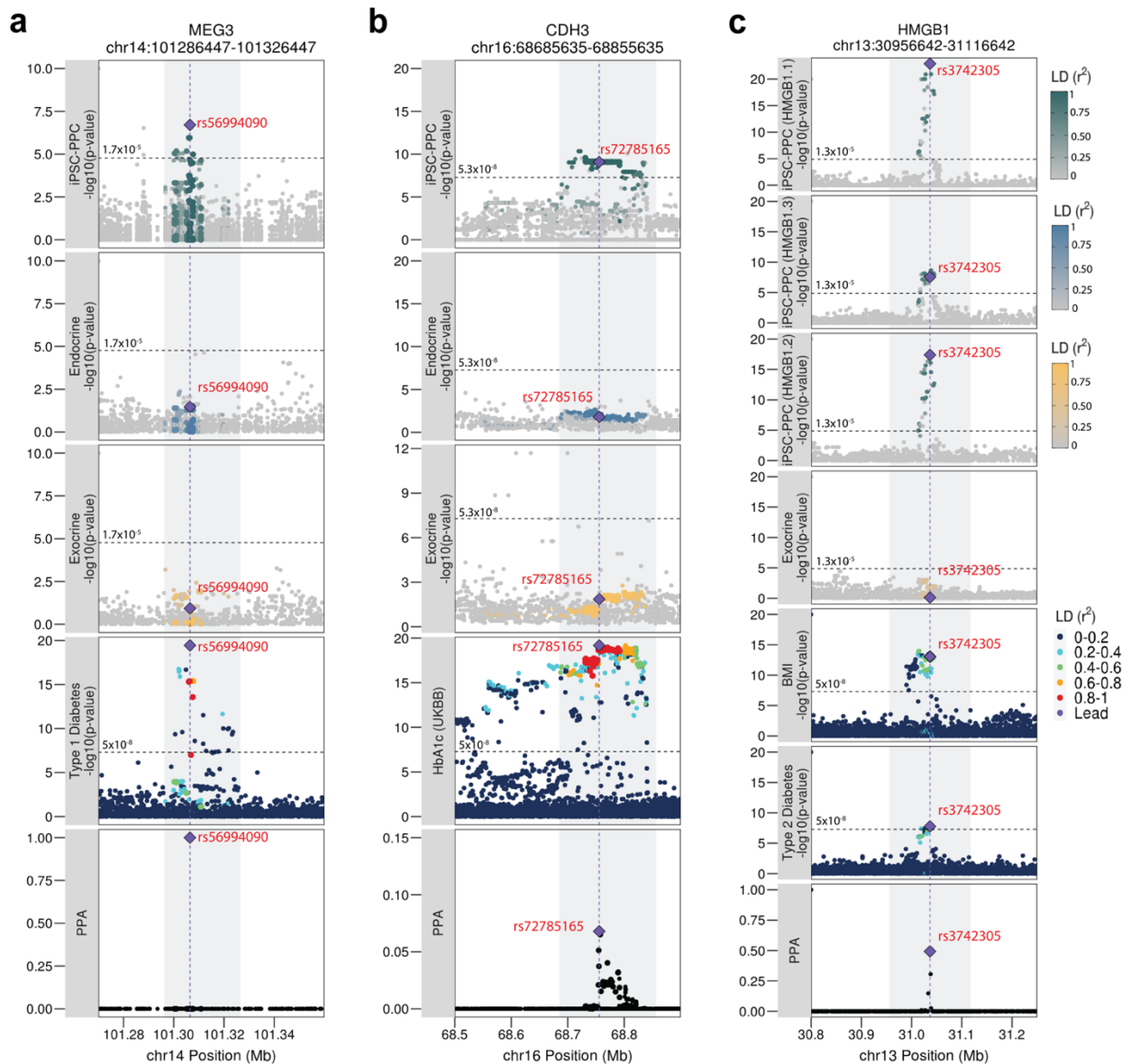


1054

1055 (a) The TPD52 locus is associated with fasting glucose levels and colocalized with an iPSC-PPC-unique
 1056 e_g QTL with the predicted causal variant identified as rs12549167 (chr8:81078464:C>T, PP = 33.9%). (b) The
 1057 CDC37L1-DT locus is associated with fasting glucose and type 1 diabetes and colocalized with an iPSC-PPC-unique
 1058 singleton e_g QTL with the predicted causal variant identified as rs10758593 (chr9:4292083:G>A, PP = 79.2%). (c)
 1059 Cholesterol and LDL direct GWAS loci colocalize with a fetal-adult e_g QTL module where the variants are associated
 1060 with *ADSL* expression in iPSC-PPC and *ST13* expression in the adult tissues. The predicted causal variant was
 1061 identified as rs138349 (chr22:41249522:A>G, PP = 21.9%). For plotting purposes, we assigned a single p-value for
 1062 gene-level significance based on Bonferroni-correction (0.05 divided by the number of variants tested for the gene;
 1063 horizontal line). Red vertical lines indicate the positions of the lead candidate causal variants underlying the
 1064 colocalization based on maximum PP.

1065

Figure 7. Pancreatic GWAS Associations with Fetal-specific Alternative Splicing



1066

1067 (a) T1D-risk locus colocalized with an iPSC-PPC-unique singleton $e_{AS}QTL$ for *MEG3* with the predicted causal variant
 1068 identified as rs56994090 (chr14:101306447:T>C, PP = 100%). (b) GWAS locus associated with HbA1c colocalized
 1069 with an iPSC-PPC-unique singleton $e_{AS}QTL$ for *CDH3* with the predicted causal variant identified as rs72785165
 1070 (chr16:68755635:T>A, PP = 6.8%). (c) *HMGB1* locus was associated with T2D-risk and BMI and colocalized with an
 1071 iPSC-PPC-unique $e_{AS}QTL$ module for differential usage of three *HMGB1* isoforms with the predicted causal variant
 1072 identified as rs3742305 (chr13:31036642:C>G, PP = 49.3%). For plotting purposes, we assigned a single p-value
 1073 for gene-level significance based on Bonferroni-correction (0.05 divided by the number of variants tested for the gene;
 1074 horizontal line). Red vertical lines indicate the positions of the lead candidate causal variants underlying the
 1075 colocalization based on maximum PP.

1076 **References**

- 1077 1. Broad Genomics Platform, DiscovEHR Collaboration, CHARGE, et al. Exome sequencing of 20,791 cases of
1078 type 2 diabetes and 24,440 controls. *Nature*. 2019;570(7759):71-76. doi:10.1038/s41586-019-1231-2
- 1079 2. Chen J, Spracklen CN, Marenne G, et al. The trans-ancestral genomic architecture of glycaemic traits. *Nat Genet*.
1080 2021;53(6):840-860. doi:10.1038/s41588-021-00852-9
- 1081 3. Chiou J, Geusz RJ, Okino ML, et al. Interpreting type 1 diabetes risk with genetics and single-cell epigenomics.
1082 *Nature*. 2021;594(7863):398-402. doi:10.1038/s41586-021-03552-w
- 1083 4. Mahajan A, Taliun D, Thurner M, et al. Fine-mapping type 2 diabetes loci to single-variant resolution using high-
1084 density imputation and islet-specific epigenome maps. *Nat Genet*. 2018;50(11):1505-1513. doi:10.1038/s41588-
1085 018-0241-6
- 1086 5. Ernst J, Kheradpour P, Mikkelsen TS, et al. Mapping and analysis of chromatin state dynamics in nine human
1087 cell types. *Nature*. 2011;473(7345):43-49. doi:10.1038/nature09906
- 1088 6. Maurano MT, Humbert R, Rynes E, et al. Systematic Localization of Common Disease-Associated Variation in
1089 Regulatory DNA. *Science*. 2012;337(6099):1190-1195. doi:10.1126/science.1222794
- 1090 7. Roadmap Epigenomics Consortium, Kundaje A, Meuleman W, et al. Integrative analysis of 111 reference human
1091 epigenomes. *Nature*. 2015;518(7539):317-330. doi:10.1038/nature14248
- 1092 8. GTEx Consortium. Genetic effects on gene expression across human tissues. *Nature*. 2017;550(7675):204-213.
1093 doi:10.1038/nature24277
- 1094 9. Kim-Hellmuth S, Aguet F, Oliva M, et al. Cell type-specific genetic regulation of gene expression across human
1095 tissues. *Science*. 2020;369(6509):eaaz8528. doi:10.1126/science.aaz8528
- 1096 10. The GTEx Consortium. The GTEx Consortium atlas of genetic regulatory effects across human tissues. *Science*.
1097 2020;369(6509):1318-1330. doi:10.1126/science.aaz1776
- 1098 11. Viñuela A, Varshney A, van de Bunt M, et al. Genetic variant effects on gene expression in human pancreatic
1099 islets and their implications for T2D. *Nat Commun*. 2020;11(1):4912. doi:10.1038/s41467-020-18581-8
- 1100 12. D'Antonio M, Arthur TD, Nguyen JP, Matsui H, D'Antonio-Chronowska A, Frazer KA. *Fine Mapping*
1101 *Spatiotemporal Mechanisms of Genetic Variants Underlying Cardiac Traits and Disease*. *Genetics*; 2022.
1102 doi:10.1101/2021.09.01.458619

- 1103 13. Strober BJ, Elorbany R, Rhodes K, et al. Dynamic genetic regulation of gene expression during cellular
1104 differentiation. *Science*. 2019;364(6447):1287-1290. doi:10.1126/science.aaw0040
- 1105 14. Dabelea D, Pettitt DJ. Intrauterine Diabetic Environment Confers Risks for Type 2 Diabetes Mellitus and Obesity
1106 in the Offspring, in Addition to Genetic Susceptibility. *Journal of Pediatric Endocrinology and Metabolism*.
1107 2001;14(8). doi:10.1515/jpem-2001-0803
- 1108 15. Petersen MBK, Gonçalves CAC, Kim YH, Grapin-Botton A. Recapitulating and Deciphering Human Pancreas
1109 Development From Human Pluripotent Stem Cells in a Dish. In: *Current Topics in Developmental Biology*. Vol
1110 129. Elsevier; 2018:143-190. doi:10.1016/bs.ctdb.2018.02.009
- 1111 16. Travers ME, Mackay DJG, Dekker Nitert M, et al. Insights Into the Molecular Mechanism for Type 2 Diabetes
1112 Susceptibility at the *KCNQ1* Locus From Temporal Changes in Imprinting Status in Human Islets. *Diabetes*.
1113 2013;62(3):987-992. doi:10.2337/db12-0819
- 1114 17. Zhao J, Bradfield JP, Zhang H, et al. Examination of All Type 2 Diabetes GWAS Loci Reveals *HHEX-IDE* as a
1115 Locus Influencing Pediatric BMI. *Diabetes*. 2010;59(3):751-755. doi:10.2337/db09-0972
- 1116 18. Colclough K, Bellanne-Chantelot C, Saint-Martin C, Flanagan SE, Ellard S. Mutations in the Genes Encoding
1117 the Transcription Factors Hepatocyte Nuclear Factor 1 Alpha and 4 Alpha in Maturity-Onset Diabetes of the
1118 Young and Hyperinsulinemic Hypoglycemia. *Human Mutation*. 2013;34(5):669-685. doi:10.1002/humu.22279
- 1119 19. Hansen L, Urioste S, Petersen HV, et al. Missense Mutations in the Human Insulin Promoter Factor-1 Gene and
1120 Their Relation to Maturity-Onset Diabetes of the Young and Late-Onset Type 2 Diabetes Mellitus in
1121 Caucasians*. *The Journal of Clinical Endocrinology & Metabolism*. 2000;85(3):1323-1326.
1122 doi:10.1210/jcem.85.3.6421
- 1123 20. Sanyoura M, Philipson LH, Naylor R. Monogenic Diabetes in Children and Adolescents: Recognition and
1124 Treatment Options. *Curr Diab Rep*. 2018;18(8):58. doi:10.1007/s11892-018-1024-2
- 1125 21. Geusz RJ, Wang A, Chiou J, et al. Pancreatic progenitor epigenome maps prioritize type 2 diabetes risk genes
1126 with roles in development. *eLife*. 2021;10:e59067. doi:10.7554/eLife.59067
- 1127 22. Ameri J, Borup R, Prawiro C, et al. Efficient Generation of Glucose-Responsive Beta Cells from Isolated GP2 +
1128 Human Pancreatic Progenitors. *Cell Reports*. 2017;19(1):36-49. doi:10.1016/j.celrep.2017.03.032
- 1129 23. Gonçalves CA, Larsen M, Jung S, et al. A 3D system to model human pancreas development and its reference
1130 single-cell transcriptome atlas identify signaling pathways required for progenitor expansion. *Nat Commun*.
1131 2021;12(1):3144. doi:10.1038/s41467-021-23295-6

- 1132 24. Nostro MC, Sarangi F, Yang C, et al. Efficient Generation of NKX6-1+ Pancreatic Progenitors from Multiple
1133 Human Pluripotent Stem Cell Lines. *Stem Cell Reports*. 2015;4(4):591-604. doi:10.1016/j.stemcr.2015.02.017
- 1134 25. Pagliuca FW, Millman JR, Gürtler M, et al. Generation of Functional Human Pancreatic β Cells In Vitro. *Cell*.
1135 2014;159(2):428-439. doi:10.1016/j.cell.2014.09.040
- 1136 26. Rezanian A, Bruin JE, Arora P, et al. Reversal of diabetes with insulin-producing cells derived in vitro from human
1137 pluripotent stem cells. *Nat Biotechnol*. 2014;32(11):1121-1133. doi:10.1038/nbt.3033
- 1138 27. Russ HA, Parent AV, Ringler JJ, et al. Controlled induction of human pancreatic progenitors produces functional
1139 beta-like cells *in vitro*. *EMBO J*. 2015;34(13):1759-1772. doi:10.15252/embj.201591058
- 1140 28. Jin W, Jiang W. Stepwise differentiation of functional pancreatic β cells from human pluripotent stem cells. *Cell*
1141 *Regen*. 2022;11(1):24. doi:10.1186/s13619-022-00125-8
- 1142 29. DeBoever C, Li H, Jakubosky D, et al. Large-Scale Profiling Reveals the Influence of Genetic Variation on Gene
1143 Expression in Human Induced Pluripotent Stem Cells. *Cell Stem Cell*. 2017;20(4):533-546.e7.
1144 doi:10.1016/j.stem.2017.03.009
- 1145 30. Panopoulos AD, D'Antonio M, Benaglio P, et al. iPSCORE: A Resource of 222 iPSC Lines Enabling Functional
1146 Characterization of Genetic Variation across a Variety of Cell Types. *Stem Cell Reports*. 2017;8(4):1086-1100.
1147 doi:10.1016/j.stemcr.2017.03.012
- 1148 31. Fadista J, Vikman P, Laakso EO, et al. Global genomic and transcriptomic analysis of human pancreatic islets
1149 reveals novel genes influencing glucose metabolism. *Proc Natl Acad Sci USA*. 2014;111(38):13924-13929.
1150 doi:10.1073/pnas.1402665111
- 1151 32. GTEx Consortium. The Genotype-Tissue Expression (GTEx) project. *Nat Genet*. 2013;45(6):580-585.
1152 doi:10.1038/ng.2653
- 1153 33. Veres A, Faust AL, Bushnell HL, et al. Charting cellular identity during human in vitro β -cell differentiation.
1154 *Nature*. 2019;569(7756):368-373. doi:10.1038/s41586-019-1168-5
- 1155 34. Jansen R, Hottenga JJ, Nivard MG, et al. Conditional eQTL analysis reveals allelic heterogeneity of gene
1156 expression. *Hum Mol Genet*. 2017;26(8):1444-1451. doi:10.1093/hmg/ddx043
- 1157 35. Giambartolomei C, Vukcevic D, Schadt EE, et al. Bayesian Test for Colocalisation between Pairs of Genetic
1158 Association Studies Using Summary Statistics. Williams SM, ed. *PLoS Genet*. 2014;10(5):e1004383.
1159 doi:10.1371/journal.pgen.1004383

- 1160 36. Yan J, Qiu Y, Ribeiro dos Santos AM, et al. Systematic analysis of binding of transcription factors to noncoding
1161 variants. *Nature*. 2021;591(7848):147-151. doi:10.1038/s41586-021-03211-0
- 1162 37. Garrido-Martín D, Borsari B, Calvo M, Reverter F, Guigó R. Identification and analysis of splicing quantitative
1163 trait loci across multiple tissues in the human genome. *Nat Commun*. 2021;12(1):727. doi:10.1038/s41467-020-
1164 20578-2
- 1165 38. van de Bunt M, Manning Fox JE, Dai X, et al. Transcript Expression Data from Human Islets Links Regulatory
1166 Signals from Genome-Wide Association Studies for Type 2 Diabetes and Glycemic Traits to Their Downstream
1167 Effectors. Stranger BE, ed. *PLoS Genet*. 2015;11(12):e1005694. doi:10.1371/journal.pgen.1005694
- 1168 39. Chen JH, Zhao Y, Khan RAW, et al. SNX29, a new susceptibility gene shared with major mental disorders in
1169 Han Chinese population. *The World Journal of Biological Psychiatry*. 2021;22(7):526-534.
1170 doi:10.1080/15622975.2020.1845793
- 1171 40. Anderson D, Cordell HJ, Fakiola M, et al. First genome-wide association study in an Australian aboriginal
1172 population provides insights into genetic risk factors for body mass index and type 2 diabetes. *PLoS One*.
1173 2015;10(3):e0119333. doi:10.1371/journal.pone.0119333
- 1174 41. Gorkin DU, Barozzi I, Zhao Y, et al. An atlas of dynamic chromatin landscapes in mouse fetal development.
1175 *Nature*. 2020;583(7818):744-751. doi:10.1038/s41586-020-2093-3
- 1176 42. Dixon JR, Jung I, Selvaraj S, et al. Chromatin architecture reorganization during stem cell differentiation. *Nature*.
1177 2015;518(7539):331-336. doi:10.1038/nature14222
- 1178 43. Chen C, Yu W, Tober J, et al. Spatial Genome Re-organization between Fetal and Adult Hematopoietic Stem
1179 Cells. *Cell Reports*. 2019;29(12):4200-4211.e7. doi:10.1016/j.celrep.2019.11.065
- 1180 44. Frankish A, Diekhans M, Ferreira AM, et al. GENCODE reference annotation for the human and mouse genomes.
1181 *Nucleic Acids Research*. 2019;47(D1):D766-D773. doi:10.1093/nar/gky955
- 1182 45. Thurner M, van de Bunt M, Torres JM, et al. Integration of human pancreatic islet genomic data refines regulatory
1183 mechanisms at Type 2 Diabetes susceptibility loci. *eLife*. 2018;7:e31977. doi:10.7554/eLife.31977
- 1184 46. Pan-UKB team. Published online 2020. <https://pan.ukbb.broadinstitute.org>
- 1185 47. Dimas AS, Lagou V, Barker A, et al. Impact of Type 2 Diabetes Susceptibility Variants on Quantitative Glycemic
1186 Traits Reveals Mechanistic Heterogeneity. *Diabetes*. 2014;63(6):2158-2171. doi:10.2337/db13-0949

- 1187 48. Grarup N, Sandholt CH, Hansen T, Pedersen O. Genetic susceptibility to type 2 diabetes and obesity: from
1188 genome-wide association studies to rare variants and beyond. *Diabetologia*. 2014;57(8):1528-1541.
1189 doi:10.1007/s00125-014-3270-4
- 1190 49. Baralle FE, Giudice J. Alternative splicing as a regulator of development and tissue identity. *Nat Rev Mol Cell*
1191 *Biol*. 2017;18(7):437-451. doi:10.1038/nrm.2017.27
- 1192 50. D'Antonio M, Nguyen JP, Arthur TD, et al. In heart failure reactivation of RNA-binding proteins is associated
1193 with the expression of 1,523 fetal-specific isoforms. Zhang Z, ed. *PLoS Comput Biol*. 2022;18(2):e1009918.
1194 doi:10.1371/journal.pcbi.1009918
- 1195 51. Mazin PV, Khaitovich P, Cardoso-Moreira M, Kaessmann H. Alternative splicing during mammalian organ
1196 development. *Nat Genet*. 2021;53(6):925-934. doi:10.1038/s41588-021-00851-w
- 1197 52. Brun T, Jiménez-Sánchez C, Madsen JGS, et al. AMPK Profiling in Rodent and Human Pancreatic Beta-Cells
1198 under Nutrient-Rich Metabolic Stress. *IJMS*. 2020;21(11):3982. doi:10.3390/ijms21113982
- 1199 53. Minokoshi Y, Alquier T, Furukawa N, et al. AMP-kinase regulates food intake by responding to hormonal and
1200 nutrient signals in the hypothalamus. *Nature*. 2004;428(6982):569-574. doi:10.1038/nature02440
- 1201 54. Shaw RJ, Lamia KA, Vasquez D, et al. The Kinase LKB1 Mediates Glucose Homeostasis in Liver and
1202 Therapeutic Effects of Metformin. *Science*. 2005;310(5754):1642-1646. doi:10.1126/science.1120781
- 1203 55. Yamauchi T, Kamon J, Minokoshi Y, et al. Adiponectin stimulates glucose utilization and fatty-acid oxidation
1204 by activating AMP-activated protein kinase. *Nat Med*. 2002;8(11):1288-1295. doi:10.1038/nm788
- 1205 56. Wu Y, Viana M, Thirumangalathu S, Loeken MR. AMP-activated protein kinase mediates effects of oxidative
1206 stress on embryo gene expression in a mouse model of diabetic embryopathy. *Diabetologia*. 2012;55(1):245-254.
1207 doi:10.1007/s00125-011-2326-y
- 1208 57. Grant SFA, Qu HQ, Bradfield JP, et al. Follow-Up Analysis of Genome-Wide Association Data Identifies Novel
1209 Loci for Type 1 Diabetes. *Diabetes*. 2009;58(1):290-295. doi:10.2337/db08-1022
- 1210 58. the DIAbetes Genetics Replication And Meta-analysis (DIAGRAM) Consortium, Morris AP, Voight BF, et al.
1211 Large-scale association analysis provides insights into the genetic architecture and pathophysiology of type 2
1212 diabetes. *Nat Genet*. 2012;44(9):981-990. doi:10.1038/ng.2383
- 1213 59. Kang HS, Kim YS, ZeRuth G, et al. Transcription Factor Glis3, a Novel Critical Player in the Regulation of
1214 Pancreatic β -Cell Development and Insulin Gene Expression. *Mol Cell Biol*. 2009;29(24):6366-6379.
1215 doi:10.1128/MCB.01259-09

- 1216 60. Kang HS, Takeda Y, Jeon K, Jetten AM. The Spatiotemporal Pattern of Glis3 Expression Indicates a Regulatory
1217 Function in Bipotent and Endocrine Progenitors during Early Pancreatic Development and in Beta, PP and Ductal
1218 Cells. Blondeau B, ed. *PLoS ONE*. 2016;11(6):e0157138. doi:10.1371/journal.pone.0157138
- 1219 61. Yang Y, Chang BH, Chan L. Sustained expression of the transcription factor GLIS3 is required for normal beta
1220 cell function in adults. *EMBO Mol Med*. 2013;5(1):92-104. doi:10.1002/emmm.201201398
- 1221 62. Sams EI, Ng JK, Tate V, et al. From karyotypes to precision genomics in 9p deletion and duplication syndromes.
1222 *Human Genetics and Genomics Advances*. 2022;3(1):100081. doi:10.1016/j.xhgg.2021.100081
- 1223 63. Aylward A, Chiou J, Okino ML, Kadakia N, Gaulton KJ. Shared genetic risk contributes to type 1 and type 2
1224 diabetes etiology. *Human Molecular Genetics*. Published online November 7, 2018. doi:10.1093/hmg/ddy314
- 1225 64. Graham SE, Clarke SL, Wu KHH, et al. The power of genetic diversity in genome-wide association studies of
1226 lipids. *Nature*. 2021;600(7890):675-679. doi:10.1038/s41586-021-04064-3
- 1227 65. Cao R chang, Yang W jun, Xiao W, et al. St13 protects against disordered acinar cell arachidonic acid pathway
1228 in chronic pancreatitis. *J Transl Med*. 2022;20(1):218. doi:10.1186/s12967-022-03413-8
- 1229 66. Barrett JC, Clayton DG, Concannon P, et al. Genome-wide association study and meta-analysis find that over 40
1230 loci affect risk of type 1 diabetes. *Nat Genet*. 2009;41(6):703-707. doi:10.1038/ng.381
- 1231 67. Tong Z, Fan Y, Zhang W, et al. Pancreas-specific Pten deficiency causes partial resistance to diabetes and
1232 elevated hepatic AKT signaling. *Cell Res*. 2009;19(6):710-719. doi:10.1038/cr.2009.42
- 1233 68. Wong H, Schotz MC. The lipase gene family. *Journal of Lipid Research*. 2002;43(7):993-999.
1234 doi:10.1194/jlr.R200007-JLR200
- 1235 69. Gaertner B, van Heesch S, Schneider-Lunitz V, et al. A human ESC-based screen identifies a role for the
1236 translated lncRNA LINC00261 in pancreatic endocrine differentiation. *eLife*. 2020;9:e58659.
1237 doi:10.7554/eLife.58659
- 1238 70. Chang W wei, Zhang L, Yao X ming, et al. Upregulation of long non-coding RNA MEG3 in type 2 diabetes
1239 mellitus complicated with vascular disease: a case-control study. *Mol Cell Biochem*. 2020;473(1-2):93-99.
1240 doi:10.1007/s11010-020-03810-x
- 1241 71. Kameswaran V, Bramswig NC, McKenna LB, et al. Epigenetic Regulation of the DLK1-MEG3 MicroRNA
1242 Cluster in Human Type 2 Diabetic Islets. *Cell Metabolism*. 2014;19(1):135-145. doi:10.1016/j.cmet.2013.11.016

- 1243 72. Kameswaran V, Golson ML, Ramos-Rodríguez M, et al. The Dysregulation of the *DLKI - MEG3* Locus in Islets
1244 From Patients With Type 2 Diabetes Is Mimicked by Targeted Epimutation of Its Promoter With TALE-DNMT
1245 Constructs. *Diabetes*. 2018;67(9):1807-1815. doi:10.2337/db17-0682
- 1246 73. Onengut-Gumuscu S, Chen WM, Burren O, et al. Fine mapping of type 1 diabetes susceptibility loci and evidence
1247 for colocalization of causal variants with lymphoid gene enhancers. *Nat Genet*. 2015;47(4):381-386.
1248 doi:10.1038/ng.3245
- 1249 74. Chen J, Liu Y, Min J, et al. Alternative splicing of lncRNAs in human diseases. *Am J Cancer Res*.
1250 2021;11(3):624-639.
- 1251 75. Wheeler E, Leong A, Liu CT, et al. Impact of common genetic determinants of Hemoglobin A1c on type 2
1252 diabetes risk and diagnosis in ancestrally diverse populations: A transethnic genome-wide meta-analysis. *PLoS*
1253 *Med*. 2017;14(9):e1002383. doi:10.1371/journal.pmed.1002383
- 1254 76. Parnaud G, Lavallard V, Bedat B, et al. Cadherin engagement improves insulin secretion of single human β -cells.
1255 *Diabetes*. 2015;64(3):887-896. doi:10.2337/db14-0257
- 1256 77. Pulit SL, Stoneman C, Morris AP, et al. Meta-analysis of genome-wide association studies for body fat
1257 distribution in 694 649 individuals of European ancestry. *Hum Mol Genet*. 2019;28(1):166-174.
1258 doi:10.1093/hmg/ddy327
- 1259 78. Sakaue S, Kanai M, Tanigawa Y, et al. A cross-population atlas of genetic associations for 220 human
1260 phenotypes. *Nat Genet*. 2021;53(10):1415-1424. doi:10.1038/s41588-021-00931-x
- 1261 79. Vujkovic M, Keaton JM, Lynch JA, et al. Discovery of 318 new risk loci for type 2 diabetes and related vascular
1262 outcomes among 1.4 million participants in a multi-ancestry meta-analysis. *Nat Genet*. 2020;52(7):680-691.
1263 doi:10.1038/s41588-020-0637-y
- 1264 80. Zhu Z, Guo Y, Shi H, et al. Shared genetic and experimental links between obesity-related traits and asthma
1265 subtypes in UK Biobank. *J Allergy Clin Immunol*. 2020;145(2):537-549. doi:10.1016/j.jaci.2019.09.035
- 1266 81. Calogero S, Grassi F, Aguzzi A, et al. The lack of chromosomal protein Hmg1 does not disrupt cell growth but
1267 causes lethal hypoglycaemia in newborn mice. *Nat Genet*. 1999;22(3):276-280. doi:10.1038/10338
- 1268 82. Wang Y, Zhong J, Zhang X, et al. The Role of HMGB1 in the Pathogenesis of Type 2 Diabetes. *J Diabetes Res*.
1269 2016;2016:2543268. doi:10.1155/2016/2543268
- 1270 83. Zhang K, Hocker JD, Miller M, et al. A single-cell atlas of chromatin accessibility in the human genome. *Cell*.
1271 2021;184(24):5985-6001.e19. doi:10.1016/j.cell.2021.10.024

- 1272 84. Ong C, Corces VG. Enhancers: emerging roles in cell fate specification. *EMBO Rep.* 2012;13(5):423-430.
1273 doi:10.1038/embor.2012.52
- 1274 85. Su CH, D D, Tarn WY. Alternative Splicing in Neurogenesis and Brain Development. *Front Mol Biosci.*
1275 2018;5:12. doi:10.3389/fmolb.2018.00012
- 1276 86. Urbut SM, Wang G, Carbonetto P, Stephens M. Flexible statistical methods for estimating and testing effects in
1277 genomic studies with multiple conditions. *Nat Genet.* 2019;51(1):187-195. doi:10.1038/s41588-018-0268-8
- 1278 87. Israel MA, Yuan SH, Bardy C, et al. Probing sporadic and familial Alzheimer's disease using induced pluripotent
1279 stem cells. *Nature.* 2012;482(7384):216-220. doi:10.1038/nature10821
- 1280 88. D'Antonio-Chronowska A, D'Antonio M, Frazer K. In vitro Differentiation of Human iPSC-derived
1281 Cardiovascular Progenitor Cells (iPSC-CVPCs). *Bio-Protocol.* 2020;10(18):1-43. doi:10.21769/bioprotoc.3755
- 1282 89. Danecek P, Bonfield JK, Liddle J, et al. Twelve years of SAMtools and BCFtools. *GigaScience.* 2021;10(2):1-4.
1283 doi:10.1093/gigascience/giab008
- 1284 90. D'Antonio-Chronowska A, Donovan MKR, Young Greenwald WW, et al. Association of Human iPSC Gene
1285 Signatures and X Chromosome Dosage with Two Distinct Cardiac Differentiation Trajectories. *Stem Cell*
1286 *Reports.* 2019;13(5):924-938. doi:10.1016/j.stemcr.2019.09.011
- 1287 91. Dobin A, Davis CA, Schlesinger F, et al. STAR: Ultrafast universal RNA-seq aligner. *Bioinformatics.*
1288 2013;29(1):15-21. doi:10.1093/bioinformatics/bts635
- 1289 92. Harrow J, Frankish A, Gonzalez JM, et al. GENCODE: The reference human genome annotation for the
1290 ENCODE project. *Genome Research.* 2012;22(9):1760-1774. doi:10.1101/gr.135350.111
- 1291 93. Shaun Purcell CC. PLINK 1.9.0.
- 1292 94. The 1000 Genomes Project Consortium, Corresponding authors, Auton A, et al. A global reference for human
1293 genetic variation. *Nature.* 2015;526(7571):68-74. doi:10.1038/nature15393
- 1294 95. Danecek P, McCarthy SA, HipSci Consortium, Durbin R. A Method for Checking Genomic Integrity in Cultured
1295 Cell Lines from SNP Genotyping Data. *PLoS One.* 2016;11(5):e0155014. doi:10.1371/journal.pone.0155014
- 1296 96. Li H. A statistical framework for SNP calling, mutation discovery, association mapping and population genetical
1297 parameter estimation from sequencing data. *Bioinformatics.* 2011;27(21):2987-2993.
1298 doi:10.1093/bioinformatics/btr509

- 1299 97. Li B, Dewey CN. RSEM: accurate transcript quantification from RNA-Seq data with or without a reference
1300 genome. *BMC Bioinformatics*. Published online 2011. doi:10.1201/b16589
- 1301 98. Trapnell C, Cacchiarelli D, Grimsby J, et al. The dynamics and regulators of cell fate decisions are revealed by
1302 pseudotemporal ordering of single cells. *Nat Biotechnol*. 2014;32(4):381-386. doi:10.1038/nbt.2859
- 1303 99. Kang HM, Subramaniam M, Targ S, et al. Multiplexed droplet single-cell RNA-sequencing using natural genetic
1304 variation. *Nat Biotechnol*. 2018;36(1):89-94. doi:10.1038/nbt.4042
- 1305 100. Veres A, Faust AL, Bushnell HL, et al. Charting cellular identity during human in vitro β -cell differentiation.
1306 *Nature*. 2019;569(7756):368-373. doi:10.1038/s41586-019-1168-5
- 1307 101. Butler A, Hoffman P, Smibert P, Papalexi E, Satija R. Integrating single-cell transcriptomic data across different
1308 conditions, technologies, and species. *Nat Biotechnol*. 2018;36(5):411-420. doi:10.1038/nbt.4096
- 1309 102. Casale FP, Rakitsch B, Lippert C, Stegle O. Efficient set tests for the genetic analysis of correlated traits. *Nat*
1310 *Methods*. 2015;12(8):755-758. doi:10.1038/nmeth.3439
- 1311 103. Huang QQ, Ritchie SC, Brozynska M, Inouye M. Power, false discovery rate and Winner's Curse in eQTL
1312 studies. *Nucleic Acids Research*. 2018;46(22):e133-e133. doi:10.1093/nar/gky780
- 1313 104. Van Nostrand EL, Pratt GA, Shishkin AA, et al. Robust transcriptome-wide discovery of RNA-binding protein
1314 binding sites with enhanced CLIP (eCLIP). *Nat Methods*. 2016;13(6):508-514. doi:10.1038/nmeth.3810
- 1315 105. Lee D, Gorkin DU, Baker M, et al. A method to predict the impact of regulatory variants from DNA sequence.
1316 *Nat Genet*. 2015;47(8):955-961. doi:10.1038/ng.3331
- 1317 106. Csardi, Gabor N Tamas. The igraph software package for complex network research. *InterJournal*. 2006;Complex
1318 Systems:1695.
- 1319 107. Mahajan A, Taliun D, Thurner M, et al. Fine-mapping type 2 diabetes loci to single-variant resolution using high-
1320 density imputation and islet-specific epigenome maps. *Nature Genetics*. 2018;50(11):1505-1513.
1321 doi:10.1038/s41588-018-0241-6
- 1322 108. Chen J, Spracklen CN, Marenne G, et al. The trans-ancestral genomic architecture of glycaemic traits. *Nature*
1323 *Genetics*. 2021;53(6):840-860. doi:10.1038/s41588-021-00852-9
- 1324 109. Bioconductor Package Maintainer. liftOver: Changing genomic coordinate systems with rtracklayer::liftOver.
1325 Published online 2022.

